Transition-Metal Nanocluster Stabilization Fundamental Studies: Hydrogen Phosphate as a Simple, Effective, Readily Available, Robust, and Previously Unappreciated Stabilizer for Well-Formed, Isolable, and Redissolvable Ir(0) and Other Transition-Metal Nanoclusters

Saim Özkar† and Richard G. Finke*,‡

Contribution from Department of Chemistry, Colorado State University, Fort Collins, Colorado 80523, and Department of Chemistry, Middle East Technical University, 06531 Ankara, Turkey

Received September 3, 2002. In Final Form: May 9, 2003

This work tests the hypothesis that tridentate oxoanions are especially effective stabilizers of transition-metal nanoclusters when the O−O distance of the anions matches closely the M−M (M = metal) distance atop the nanocluster surface. Specifically, we test the hypothesis that HPO_4^{2-} with its 2.5 Å O−O distance is a very simple, effective, but previously unrecognized anion for the stabilization of transition-metal(0) nanoclusters such as those of Ir(0), where the Ir−Ir surface distance is ca. 2.6−2.7 Å. This hypothesis is tested by the five criteria we recently developed. These criteria emphasize the ability of a given nanocluster-stabilizing anion to allow the formation of highly kinetically controlled, near-monodisperse (≤±15%) size distributions of nanoclusters and then to allow isolable and fully redissolvable nanoclusters that exhibit, once redispersed into solution, good catalytic activity and long catalytic lifetimes. The previously unknown precursor complex $\{[Bu_4N][(1,5\text{-COD})Ir{\cdot}HPO_4]\}_n$, **1**, was prepared and shown to be a preferred precursor for the reproducible formation of hydrogen phosphate- and tetrabutylammonium-stabilized transition-metal Ir(0) nanoclusters. The nanocluster formation reaction was shown to follow the slow continuous nucleation (A → B, rate constant k_1) followed by fast autocatalytic surface growth (A + B → 2B, rate constant k_2) mechanism uncovered previously; this finding was then exploited by showing that nanocluster size control could be achieved as expected by adding excess HPO_4^{2-} to lower the k_2/k_1 ratio, resulting in the formation of smaller nanoclusters. A relatively rare experimental demonstration of the balanced reaction for nanocluster formation is also provided. Proton Sponge [i.e., 1,8-bis(dimethylamino)naphthalene] is shown to be a preferred scavenger of the 1 equiv of H^+ byproduct formed from the H_2 reduction of the $(1,5\text{-COD})Ir(I)^+$ moiety in the nanocluster precursor to Ir(0) plus H^+; positive effects of Proton Sponge on the resultant nanocluster catalytic lifetime are also demonstrated. Transmission electron microscopy (TEM) of the postcatalysis nanoclusters shows that agglomeration is a catalysis-inhibiting deactivation reaction. Overall, the results show that HPO_4^{2-} is an effective anion for the formation, and then stabilization, of Ir(0) transition-metal nanoclusters in acetone and with Bu_4N^+ countercations. More specifically, HPO_4^{2-} rates alongside citrate^{3-} in the developing series of anion efficacy for nanocluster formation, stabilization and catalytic activity: polyoxoanions > HPO_4^{2-} ∼ citrate^{3-} > other commonly employed nanocluster-stabilizing anions. Since a reasonable match between the tridentate O−O distance in HPO_4^{2-} and the M−M distances is present for the metals Fe, Co, Ni, Ru, Rh Ir, Pd, Re, Os, and Pt [i.e., the lattice size-matching criterion is fulfilled; Özkar, S.; Finke, R. G. *Coord. Chem. Rev.* **2003** (submitted for publication)], our results imply that HPO_4^{2-} merits consideration for nanocluster synthesis and stabilization any time M(0) nanoclusters of the above list of metals are planned. The additional advantages of HPO_4^{2-} are also presented and briefly discussed, namely, its thermal robustness, its high resistance to reduction or oxidation, its valuable ^{31}P NMR handle, and its inexpensive and readily available nature. Finally, it is briefly discussed how the results provide molecular-level insight to guide the molecularly ill-understood area of phosphating of metal surfaces to achieve corrosion resistance, electrical resistance, or bonding to organic coatings such as rubber.

Introduction

In the explosively growing field of nanoparticle science,[1,2] transition-metal nanoclusters are of considerable interest for their applications in catalysis and their potential to serve as "soluble analogues of heterogeneous catalysts".[2,3] Of particular interest are near-monodisperse (≤±15% size distribution)[4] nanoclusters whose size and shape, size distribution, and composition can be reproducibly controlled via designed syntheses. Also important is that the resultant nanoclusters be stable enough to be isolable, bottleable, and fully redissolvable yet retain high catalytic activity and long lifetime when redissolved in nonaqueous solvents. Recent work has shown that the anion stabilizer coordinated to the surface of the nanocluster is a key to the stabilization of transition-metal nanoclusters[5] [see Figure 1a in ref 5a plus lead references to Derjaguin−Landau−Verway−Overbeek (DLVO) theory of colloidal stabilization].[6] That work also reveals that tridentate oxoanion ligands are especially effective anions for the kinetically controlled growth, and then high stabilization, of at least Ir(0) nanoclusters.[5]

In an unprecedented molecular-level structural insight into what factors give rise to the best anionic stabilizers,[5c] a study of the series of tridentate oxoanion donors $P_2W_{15}Nb_3O_{62}^{9-}$ and $SiW_9Nb_3O_{40}^{7-}$ (e.g., polyoxoanions), $C_6H_5O_7^{3-}$ (citrate^{3-}), and $P_3O_9^{3-}$ (trimetaphosphate) re-

* To whom correspondence should be addressed.
† Middle East Technical University.
‡ Colorado State University.

10.1021/la0207522 CCC: $25.00
Published on Web 06/25/2003

vealed that the anions with the closest O−O distance match to the Ir−Ir surface distance of 2.6−2.7 Å are the best stabilizers, other factors such as basicity (and thus Ir−O σ bond energy) being taken into account.[5c] The C_3 symmetry, tridentate oxoanion, anion-to-nanocluster surface lattice size-matching model[5c] yielded several novel and testable predictions, the first of which is that simple HPO_4^{2-} with its O−O distance of 2.5 Å should be an effective, previously unrecognized[7] anion for stabilization of Ir(0) nanoclusters (as an initial test case; the Ir−Ir surface distance is 2.6−2.7 Å and thus a reasonable match for initial studies).[5c] It is precisely this first prediction of the lattice size-matching model/hypothesis that is tested in the present work. If HPO_4^{2-} is an effective anion for the kinetically controlled synthesis, and then stabilization, of Ir(0) transition-metal nanoclusters, then that finding would be both an important test of the lattice size-matching model and an important result in its own right given the other properties of HPO_4^{2-}: it is cheap, readily available, resistant to reduction[8] and oxidation, all inorganic, thermally robust,[9] and it also has a valuable ^{31}P NMR handle.

One practical issue derives from the pK_as of the three conjugate acids of PO_4^{3-}: H_3PO_4, pK_{a1} = 2.2; $H_2PO_4^-$, pK_{a2} = 7.2; and HPO_4^{2-}, pK_{a3} = 12.4. It is easily shown by simple acid−base equilibrium calculations that 3[Bu_4N]OH [conjugate acid H_2O pK_a (in water) = 15.7] is insufficient to fully deprotonate H_3PO_4, in the ca. 0.01−0.10 M concentration range of the present studies, to yield the otherwise ideally desired, most basic, and presumably most coordinating ligand, tetrabutylammonium phosphate, $[Bu_4N]_3PO_4$.[10] This is the reason the present study examines monohydrogen phosphate anion, $[Bu_4N]_2HPO_4$, as the most basic form of phosphate that is readily available.

(1) Reviews (see also elsewhere[2]): (a) Schmid, G.; Baumle, M.; Geerkens, M.; Heim, I.; Osemann, C.; Sawitowski, T. *Chem. Soc. Rev.* **1999**, *28*, 179. (b) Schmid, G.; Chi, L. F. *Adv. Mater.* **1998**, *10*, 515. (c) Fendler, J. H., Ed. *Nanoparticles and Nanostructured Films*; Wiley-VCH: Weinheim, Germany, 1998. (d) Fürstner, A., Ed. *Active Metals: Preparation, Characterization, and Applications*; VCH: Weinheim, Germany, 1996. (e) Bradley, J. S. In *Clusters and Colloids. From Theory to Applications*; Schmid, G., Ed.; VCH: New York, 1994; pp 459−544. (f) Schmid, G. *Chem. Rev.* **1992**, *92*, 1709. (g) A superb series of papers, complete with a record of the insightful comments by the experts attending the conference, is available in *Faraday Discuss.* **1991**, *92*, 1−300. (h) Schmid, G. In *Aspects of Homogeneous Catalysis*; Ugo, R., Ed.; Kluwer: Dordrecht, The Netherlands, 1990; Chapt. 1. (i) Andres, R. P.; Averback, R. S.; Brown, W. L.; Brus, L. E.; Goddard, W. A., III; Kaldor, A.; Louie, S. G.; Moscovits, M.; Peercy, P. S.; Riley, S. J.; Siegel, R. W.; Spaepen, F.; Wang, Y. *J. Mater. Res.* **1989**, *4*, 704. (j) Henglein, A. *Chem. Rev.* **1989**, *89*, 1861. (k) Thomas, J. M. *Pure Appl. Chem.* **1988**, *60*, 1517. (l) Jena, P.; Rao, B. K.; Khanna, S. N; *Physics and Chemistry of Small Clusters*; Plenum: New York, 1987.

(2) (a) Aiken, J. D., III; Finke, R. G. *J. Mol. Cat. A: Chem.* **1999**, *145*, 1. (b) Aiken, J. D., III; Lin, Y.; Finke, R. G. *J. Mol. Catal. A: Chem.* **1996**, *114*, 29−51. (c) Finke, R. G. Transition-Metal Nanoclusters: Solution-Phase Synthesis, then Characterization and Mechanism of Formation, of Polyoxoanion- and Tetrabutylammonium-Stabilized Nanoclusters. In *Metal Nanoparticles: Synthesis, Characterization and Applications*; Feldheim, D. L., Foss, C. A., Jr., Eds.; Marcel Dekker, Inc.: New York, 2002; Chapt. 2, pp 17−54.

(3) Representative recent papers on nanocluster catalysis: (a) Templeton, A. C.; Wuelfin, W. P.; Murray, R. W. *Acc. Chem. Res.* **2000**, *33*, 27. (b) Rao, C. N. R.; Kulkarni, G. U.; Thomas, P. J.; Edwards, P. P. *Chem. Soc. Rev.* **2000**, *29*, 27. (c) Schmid, G.; Baumle, M.; Geerkens, M.; Helm. I.; Osemann, C.; Sawitowski, T. *Chem. Soc. Rev.*, **1999**, *28*, 179. (d) Stein, J.; Lewis, L. N.; Gao, Y.; Scott, R. A. *J. Am. Chem. Soc.* **1999**, *121*, 3693. (e) Reetz, M. T.; Breinbauer, R.; Wedemann, P.; Binger, P. *Tetrahedron* **1998**, *54*, 1233. (f) Schmidt, T. J.; Noeske, M.; Gasteiger, H. A.; Behm, R. J.; Britz, P.; Brijoux, W.; Bönnemann, H. *Langmuir* **1997**, *13*, 2591. (g) Schmid, G.; Maihack, V.; Lantermann, F.; Peschel, S. *J. Chem. Soc., Dalton Trans.* **1996**, 589. (h) Reetz, M. T.; Lohmer, J. G. *Chem. Soc., Chem. Commun.* **1996**, 1921. (i) Reetz, M. T.; Breinbauer, R.; Wanninger, K. *Tetrahedron Lett.* **1996**, *37*, 4499. (j) Reetz, M. T.; Quaiser, S. A.; Merk, C. *Chem. Ber.* **1996**, *129*, 741. (k) Bönnemann, H.; Braun, G. A. *Angew. Chem., Int. Ed. Eng.* **1996**, *35*, 1992. (l) Wilcoxon, J. P.; Martino, T.; Klavetter, E.; Sylwester, A. P. *Nanophase Mater.* **1994**, 771. (m) Lewis, L. N. *Chem. Rev.* **1993**, *93*, 2693.

(4) See elsewhere[2] for a review of nanocluster catalysis, which includes necessary key terms and definitions of nanoclusters vs traditional (nano-) colloids, monodisperse (±0% size distribution) and near-monodisperse (≤±15% size distribution) nanoparticles, "magic number" (i.e., full shell and thus enhanced stability) nanoclusters, Schwartz's updated definition of homogeneous vs heterogeneous catalysts, and inorganic (charge) and organic (steric) stabilization mechanisms for colloids and nanoparticles.

(5) (a) Özkar, S.; Finke, R. G. *J. Am. Chem Soc.* **2002**, *124*, 5796. (b) Özkar, S.; Finke, R. G. *Langmuir* **2002**, *18*, 7653. (c) See also ref 28.

(6) (a) Evans, D. F.; Wennerström, H. *The Colloidal Domain*, 2nd ed.; Wiley−VCH: New York, 1999. (b) Hirtzel, C. S.; Rajogopalan, R. *Colloidal Phenomena: Advanced Topics*; Noyes Publications: Park Ridge, NJ, 1985; pp 27−39 and 73−87. (c) Hunter, R. J. *Foundations of Colloid Science*; Oxford University Press: New York, 1987; Vol. 1, pp 316−492.

(7) A SciFinder search of the literature yielded only two reports on the use of phosphate anion to stabilize (silver) colloids;[a,b] no prior study of phosphate to stabilize modern transition-metal(0) nanoclusters[2] has appeared. Moreover, none of the prior reports provides any idea that phosphate might be a more general stabilizer with an effectiveness comparable to that of citrate^{3-}; there is also no idea in the prior literature that phosphate or hydrogen phosphate might be applicable to a broader range of metal(0) nanoclusters[29] as suggested by the results reported herein. Finally, it is even ambiguous which protonation state of phosphate is the actual stabilizer, as well as what the charge and formal oxidation state are on the surface metals, of the prior (Ag) nanocolloid work.[a,b] (a) Schneider, S.; Grau, H.; Halbig, P.; Freunscht, P.; Nickel, U. *J. Raman Spectrosc.* **1996**, *27*, 57. (b) Greaves, S. J.; Griffith, W. P. *J. Raman Spectrosc.* **1988**, *19*, 503. (c) Phosphate has also been used to stabilize $(AgI)_n$, a historically important system in which double layer theory was tested: Hunter, R. J. In *Foundations of Colloidal Science*; Oxford University Press: New York, 1987; Vol. 1, p 369; see also Van den Hul, H. J.; Lyklema, J. *J. Colloid Sci.* **1967**, *23*, 500. (d) One other paper reports the use of $Co^{II}_3(PO_4)_2$ in colloid preparation as an integral component of higher-valent metal colloids, that is, materials that obviously are not HPO_4^{2-} anion-stabilized metal(0) nanoclusters such as those made in the present work; see Ishikawa, T.; Matijevic, E. *J. Colloid Interface Sci.* **1988**, *123*, 122. (e) A recent paper adds Na_3PO_4 to serve as a base in a Pd nanocluster-catalyzed Suzuki coupling reaction but focuses only on the polymer or dendrimer stabilizers present; an unrecognized stabilizing effect due to the phosphate, as well as stabilization due to the other anions present, are probable in that work: Li, Y.; El-Sayed, M. A. *J. Phys. Chem. B* **2001**, *105*, 8938. For phosphating metal surfaces, see also: (f) Rausch, W. *The Phosphating of Metals*; Finishing Publications Ltd.: Teddington, Middlesex, England, 1990. (g) Yu, T.; Li, L.; Lin, C. T. *J. Phys. Chem.* **1995**, *99*, 7613. These authors note that "the chemical and physical fundamentals of the molecular level of metal phosphate formed at the coating interface have never been systematically studied". They propose a PO^- species to bind to the metal surface; our work in the present paper suggests, instead, PO_3^{n-} binding to the metal surface. (h) Kozlov, L. A.; Okulov, V. V. AVTOBAZ, Tolyatti, Russia. *Gal'vanotekhnika i Obrabotka Poverkhnosti*, **1999**, *7(2)*, 27−32. ("Phosphating Theory and Practice"; in Russian; CAN 132: 254222.) (i) Giles, T. R. *Metal Finishing* **2001**, *99* (9), 10−12, 14−16, 18−20. ("Pretreatment of Various Substrates Prior to Electrocoating"; Henkel Surface Technologies, Henkel Corp, Madison Heights, MI; CAN 135:306595.) (j) Schuemichen, H. Interfinish 92, Int. Congr. Surf. Finish, **1992**, *2*, 630−639. ("New Developments in the Field of Phosphating Metal Surfaces"; Publisher: Assoc. Bras. Trat. Superficie, Sao Paulo, Brazil; CAN 119: 165228.)

(8) In fact, PO_4^{3-} is special among the oxoanions of the main-group elements in not being readily reducible as judged by its large, negative standard potential, even to the next oxidation state of phosphorus, in both acidic and basic solutions ($E°$ = −0.933 and −1.12 V, respectively, versus hydrogen): Bard, A. J.; Parsons, R.; Jordan. J., Eds. *Standard Potentials in Aqueous Solution*; Marcel Dekker: New York, 1985.

(9) (a) A search of the literature revealed a single report of the reduction of transition-metal phosphates to phosphides under hydrogen, a reaction that requires very high, 850−1000 °C temperatures: Gopalakrishnan, J.; Pandey, S.; Rangan, K. K. *Chem. Mater.* **1980**, *9*, 22113. (b) In a control experiment reported in the Experimental Section herein, HPO_4^{2-} was shown to be stable under the mild conditions of our nanocluster synthesis (22 °C, 3.7 atm of H_2). Given the precedent cited above,[9a] it is expected to be stable under much more vigorous catalytic reaction conditions as well. (c) The low solubility of alkali-metal phosphate salts, especially in nonaqueous solvents, may have prevented their use previously. Fortunately, however, the tetrabutylammonium monohydrogen phosphate, $[(n\text{-}C_4H_9)_4N]_2HPO_4$, and dihydrogen phosphate, $[(n\text{-}C_4H_9)_4N]H_2PO_4$, are both soluble in polar organic solvents such as acetone and acetonitrile.

(10) Greenwood, N. N.; Earnshaw, A. *Chemistry of the Elements*; Pergamon Press, Ltd.: New York, 1984; p 598.

The results obtained are of fundamental interest to nanocluster science, notably the following findings: (i) $[Bu_4N]_2HPO_4$ is, as predicted, an effective ligand for the formation, and then stabilization, of Ir(0) nanoclusters in acetone, performing overall equivalently to the more popular citrate^{3-} anion, $[Bu_4N]_3[C_6H_5O_7^{3-}]$; (ii) Proton Sponge [i.e., 1,8-bis(dimethylamino)naphthalene] is, as suggested recently,[5b] an effective scavanger of the H^+ formed in the H_2 reduction reaction of the nanocluster precursors (see Scheme 1), a proton scavenger with minimal metal coordinating abilities and, therefore, without significant negative effects on the nanocluster nucleation and growth reactions; and (iii) the isolated complex, $\{[Bu_4N][(1,5\text{-COD})Ir{\cdot}HPO_4]\}_n$, serves as the preferred nanocluster precursor in comparison to the in situ mixture of 1:1 $[(1,5\text{-COD})Ir(NCCH_3)_2]BF_4$ and $[Bu_4N]_2HPO_4$. In addition, the results are of interest since (iv) the nanocluster formation kinetics, when compared to previous results for the popular citrate^{3-} anion, help fortify the conclusion reached earlier[5a] that citrate^{3-} has a second nanocluster nucleation pathway and, therefore, is less desirable when used both as a reductant and as a stabilizer.

Results and Discussion

Five Criteria for Kinetically Controlled Formation and Then Stabilization of Nanoclusters. The five criteria first developed[5a] and then applied[5a-c] elsewhere are the efficacy of a given additive (e.g., anions, solvent, cations, or polymers) to achieve the following: (i) The ability to exhibit the largest k_2/k_1 ratio, indicative of the greatest amount of kinetic control in the nanocluster synthesis; that is, the greatest separation of nucleation and growth in time, results that give rise to narrower size distributions. [The two rate constants refer to the slow, continuous nucleation (A → B, rate constant k_1) followed by fast autocatalytic surface growth (A + B → 2B; rate constant k_2) mechanism first elucidated elsewhere[11] for transition-metal nanocluster growth under H_2; A in the present situation is the $Ir^I(1,5\text{-COD})^+$ precursor, whatever its exact form, and B is the Ir(0) atop the growing nanocluster's surface.] (ii) The ability to exhibit TEM (transmission electron microscopy) micrographs consistent with a near-monodisperse, ≤±15% size distribution. (iii) The ability to allow isolable, and then fully redissolvable, nanoclusters (i.e., without visible formation of bulk metal). (iv) The ability to allow high catalytic activity in the *redissolved* nanoclusters. (v) The ability to allow long catalytic lifetime in the nanoclusters as measured by the total turnovers (TTOs) for the test reaction of cyclohexene hydrogenation. By use of these five criteria, the first "anion efficacy series" was obtained for the formation and stabilization of Ir(0) nanoclusters in acetone solvent and for Bu_4N^+ countercations, specifically[5a,b] $P_2W_{15}Nb_3O_{62}^{9-} \sim [(P_2W_{15}Nb_3O_{61})_2O]^{16-} \sim ([P_2W_{15}(TiOH)_3O_{\sim 59}]^{9-})_n$ ($n = 1$, 2) ~ $SiW_9Nb_3O_{40}^{7-}$ > $C_6H_5O_7^{3-}$ > $[\text{-}CH_2CH(CO_2^-)\text{-}]_n^{n-} \sim OAc^- \sim P_3O_9^{3-} \sim Cl^- \sim OH^-$. Note that the essence of this series is polyoxoanions > citrate^{3-} > other commonly used nanocluster-stabilizing anions.

Synthesis of Dihydrogen Phosphate- and Tetrabutylammonium-Stabilized, Near-Monodisperse Ir(0) Nanoclusters from the Preisolated Complex $\{[Bu_4N][(1,5\text{-COD})Ir{\cdot}HPO_4]\}_n$, 1. Our work with the compositionally well-defined precursor $[(1,5\text{-COD})Ir{\cdot}P_2W_{15}Nb_3O_{62}]^{8-}$ for making polyoxoanion-stabilized nanoclusters shows that the use of this chemically precise precursor is one key to the ≤±15% reproducibility in the size, catalytic activity, and other desired properties of the resultant Ir(0) nanoclusters.[2,11,12] One reason this is true is that this precursor controls exactly the amount of free $[(1,5\text{-COD})Ir(solvent)_2]^+$, traces of this solvated precursor having been shown to have a dramatic effect on shortening the induction period,[11a] thereby reducing the desired kinetic control over the nanocluster synthesis.[5,11] This is why we began with, and have emphasized in the present studies, the use of the compositionally well-defined nanocluster precursor complex $\{[Bu_4N][(1,5\text{-COD})Ir{\cdot}HPO_4]\}_n$, **1**. In a later section we will compare and contrast the results with preformed complex **1** to those somewhat different results obtained with the in situ mixing of $[(1,5\text{-COD})Ir(solvent)_2]BF_4$ and $[Bu_4N]_2HPO_4$, results which provide evidence that the well-defined precursor approach provides the best nanoclusters.[13]

The balanced Ir(0) nanocluster formation reactions beginning with **1** are shown in Scheme 1. Note that the 0.5 equiv of H_2 which reduces the Ir(I) component of the $Ir^I(1,5\text{-COD})^+$ in the precursor complex, **1**, to Ir(0) produces 1 equiv of H^+; hence, if this H^+ is not scavenged, then protonation of HPO_4^{2-} occurs to yield its conjugate acid, $H_2PO_4^-$, as the true stabilizer present. This is why one needs to add a base stronger than HPO_4^{2-} (conjugate acid $pK_{a2} = 7.2$) to the synthesis. Our previous work showed that Proton Sponge ($pK_a = 12.3$)[14] is a generally preferred base [5b,15] and that the stronger base $Bu_4N^+OH^-$ is useful to examine as well as a control reaction,[5b] so that these two bases will also be examined as part of the present study.

Scheme 1. Ir(0) Nanocluster Formation Reactions under H_2 from the Isolated Precursor $\{[Bu_4N][(1,5\text{-COD})Ir{\cdot}HPO_4]\}_n$ without, and with, Added Proton Sponge to Scavenge the H^+ Formed

$$\frac{1}{n}\{[(1,5\text{-}C_8H_{12})Ir{\cdot}HPO_4]^-\}_n + 2.5H_2 \rightarrow C_8H_{16} + Ir(0) + H^+ + HPO_4^{2-} \quad \text{(I)}$$

$$m\,Ir(0) \rightarrow Ir(0)_m \quad \text{(II)}$$

$$HPO_4^{2-} + H^+ \rightleftharpoons H_2PO_4^- \quad \text{(III)}$$

$$H^+ + \text{Proton Sponge} \rightleftharpoons \text{(Proton Sponge)-}H^+ \quad \text{(IV)}$$

From the hydrogen phosphate-supported iridium(I) complex[16] $\{[Bu_4N][(1,5\text{-COD})Ir{\cdot}HPO_4]\}_n$, **1**, 18 ± 4 Å $Ir(0)_n$ nanoclusters were grown according to equations in Scheme 1 by our previously developed standard conditions synthesis and concomitant cyclohexene hydrogenation

(11) (a) Watzky, M. A.; Finke, R. G. *J. Am. Chem. Soc.* **1997**, *119*, 10382 and references therein to the earlier literature of the mechanisms of nanoparticle formation. (b) Watzky, M. A.; Finke, R. G. *Chem. Mater.* **1997**, *9*, 3083. (c) Aiken, J. D., III; Finke, R. G. *J. Am. Chem. Soc.* **1998**, *120*, 9545 and references therein to diffusive agglomeration of nanoparticles. (d) See also ref 17 and references therein.

(12) (a) Lin, Y.; Finke, R. G. *J. Am. Chem. Soc.* **1994**, *116*, 8335. (b) Lin, Y.; Finke, R. G. *Inorg. Chem.* **1994**, *33*, 4891.

(13) (a) We recently found that impurities in aged bottles of Burdick and Jackson acetone solvent lead to poorer kinetic control (as measured by the k_1 and k_2 values), poorer apparent stabilization (leading to deactivated nanoclusters that do not fully form), and overall and therefore inferior nanoclusters with the $P_2W_{15}Nb_3O_{62}^{9-}$ plus $[(1,5\text{-COD})Ir(solvent)_2]BF_4$ in situ approach. Somewhat surprisingly, the preisolated, $[(1,5\text{-COD})Ir{\cdot}P_2W_{15}Nb_3O_{62}]^{8-}$ precursor to, ostensibly, the same polyoxoanion-stablized nanoclusters proved insensitive to the impurities in that same bottle of aged Burdick and Jackson solvent (L. Starkey and R. G. Finke, unpublished results). (b) Hence, we did a control showing that it is the inherent chemistry of the in situ approach that gives the difference. (c) We have seen effects due to acetone impurities before, but in that case (acetone stored over K_2CO_3, a procedure we do *not* recommend as discussed in ref 12b) we observed a hydrogenation rate increase: see Figures E−G and Table B plus the discussion provided in the Supporting Information in ref 12b.

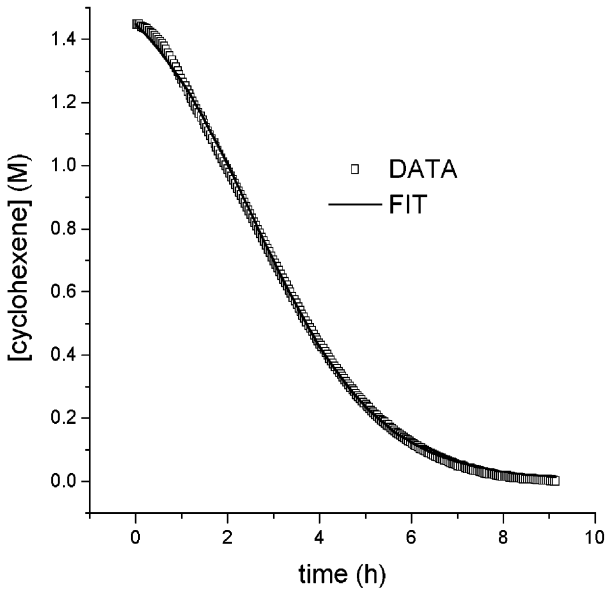

Figure 1. Typical data and curve fit of the loss of cyclohexene versus time in the hydrogenation of 1.65 M cyclohexene and concomitant formation of 18 ± 4 Å Ir(0) nanoclusters starting with 1.2 mM $\{[Bu_4N][(1,5\text{-COD})Ir{\cdot}HPO_4]\}_n$ (**1**) in acetone at 22 °C. The pressure rise in the initial part of the curve (not shown), due to the solvent vapor pressure reequilibration after 15 flushes of the reaction flask with H_2, has been corrected for (removed from this curve) by the procedure described elsewhere.[11d] A relatively small,[5a] ca. 0.5 ± 0.1 h induction period, but still an overall sigmoidal curve characteristic of autocatalysis, is seen, one well fit by the A → B and then A + B → 2B mechanism.[11]

reaction[5,12b] (i.e., 1.2 mM **1**, 40 psig of H_2, 22 °C, 1.65 M cyclohexene). Figure 1 shows the slightly sigmoidal-shaped cyclohexene vs time curve for the standard conditions reaction with its reproducible 0.5(1) h induction period. (The H_2 pressure loss is what is actually measured, but the kinetic analysis requires that the data be expressed in terms of the equivalent cyclohexene loss according to the 1:1 H_2:cyclohexene stoichiometry, as detailed elsewhere.[17]) After a short, ca. 0.5 h induction period, H_2 consumption proceeds at a roughly linear, reproducible rate of $-d[H_2]/dt = 1.0(1)$ mmol of H_2/h (when H_2 mass transfer limitations are avoided);[18] cyclohexene is hydrogenated quantitatively to cyclohexane during this time as monitored by GLC and NMR. The key data are summarized in Table 1, entry 1.

Table 1. Compilation of Data[a] for the Formation, Stabilization, and Catalytic Activity of Ir(0) Nanoclusters in the Presence of Hydrogen Phosphate and Tetrabutylammonium Cation without, or with, the Added Base Proton Sponge or Bu_4NOH

entry	precursor material	t_{ind} (h)	$-d(H_2)/dt$[b] (mmol of H_2/h)	k_1 (h^{-1})	$k_2 \times 10^{-3c}$ (M^{-1} h^{-1})	$k_2/k_1 \times 10^{-3}$	d_m[d] (Å)	appearance	redispersible?	catalytic activity[e] (mmol of H_2/h)	TTO[f]
					Preformed Precursor Method						
1	$\{[Bu_4N][(COD)Ir{\cdot}HPO_4]\}_n$	0.5(1)	1.0(1)	0.097(1)	0.66(1)	6.8(1)	18(4)	clear, yellow-brown	yes	1.0(1)	55 000
2	$\{[Bu_4N][(COD)Ir{\cdot}HPO_4]\}_n$ + 1 equiv of Proton Sponge	0.8(1)	0.8(1)	0.084(1)	0.60(1)	7.2(1)	18(4)	clear, yellow-brown	yes	0.8(1)	[150 000][g]
3	$\{[Bu_4N][(COD)Ir{\cdot}HPO_4]\}_n$ + 2 equiv of Proton Sponge	0.7(1)	0.7(1)	0.089(1)	0.56(1)	6.3(1)	21(3)	clear, yellow-brown	yes	0.9(1)	67 000
4	$\{[Bu_4N][(COD)Ir{\cdot}HPO_4]\}_n$ + 1 equiv of Bu_4NOH	2.0(2)	0.13(2)				15(4)	clear, yellow	no	0.1	
5	$\{[Bu_4N][(COD)Ir{\cdot}HPO_4]\}_n$ + 1 equiv of $[Bu_4N]_2HPO_4$	6(1)	0.20(5)				16(4)	clear, yellow-brown	yes	0.2(1)	
6	$\{[Bu_4N][(COD)Ir{\cdot}HPO_4]\}_n$ + 4 equiv of $[Bu_4N]_2HPO_4$	12(2)	0.10(5)				13(3)	clear, yellow- brown	yes	0.10(5)	
					In Situ Method						
7	$[(COD)Ir(CH_3CN)_2]BF_4 + [Bu_4N]_2HPO_4$	0.2(1)	10(1)					brown, black particles	part.	1.0(1)	
8	$[(COD)Ir(CH_3CN)_2]BF_4 + [Bu_4N]_2HPO_4$ + 1 equiv of Proton Sponge	0.2(1)	13(1)	1.61(3)	6.7(2)	4.2(1)	16(3)	clear, brown	yes	5(1)	53 000
9	$[(COD)Ir(CH_3CN)_2]BF_4 + [Bu_4N]_2HPO_4$ + 1 equiv of Bu_4NOH	0.5(1)	2.3(4)	0.083(1)	1.3(1)	16(1)	19(4)	clear, brown	yes	[0.4(1)][h]	17 800
10	$[(COD)Ir(CH_3CN)_2]BF_4 + [Bu_4N]2HPO_4$ + 2 equiv of Bu_4NOH	1.0(1)	0.26(5)	0.085(2)	0.35(1)	4.1(2)		clear, black particles	no		
11	$[(COD)Ir(CH_3CN)_2]BF_4 + [Bu_4N]H_2PO_4$	0	13(1)					clear, black particles	no		
12	$[(COD)Ir(CH_3CN)_2]BF_4 + [Bu_4N]H_2PO_4$ + 1 equiv of Proton Sponge	0	13(1)					clear, black particles	no		

[a] Each experiment in this table was repeated at least three times. [b] Note that these rates reflect the amount of $[(1,5\text{-COD})Ir]^+$ converted into active Ir(0), so that they are not readily comparable to the other entries in column and unless the induction periods are very similar so that the amount of cyclooctane evolution from the $[(1,5\text{-COD})Ir]^+$ precursor is known. [c] The k_2 values are corrected by the mathematically required stoichiometry factor of 1400 as detailed elsewhere.[11a] [d] No d_m, σ value is given if the nanocluster sample is known to be strongly contaminated with bulk metal due to the sampling error that is intrinsically present. [e] Catalytic activity is measured as the rate of hydrogenation, under standard conditions, of the Ir(0) nanoclusters, first isolated and then redispersed in acetone. [f] No TTO value is given when the nanocluster sample is known to be so strongly contaminated with bulk metal that the nanocluster contribution to the resultant TTO value would be impossible to interpret reliably. [g] TEM after the 150 000 TTOs shows considerable bulk metal; hence, this value is placed in brackets to indicate that it is an upper limit to the desired, true TTOs for the Ir(0) nanoclusters alone. [h] The low catalytic activity in this run is very likely due to the deliberate stoppage of this reaction after 7 h since we wanted to examine the nanoclusters prior to bulk metal formation (see Supporting Information for the full experimental details for this run).

(14) (a) Brzezinski, B.; Schroeder, G.; Grech, E.; Malarski, Z.; Sobczyk, L. *J. Mol. Struct.* **1992**, *274*, 75. (b) Brzezinski, B.; Glowiak, T.; Grech, E.; Malarski, Z.; Sobczyk, L. *J. Chem. Soc., Perkin Trans. 2* **1991**, 1643.

(15) On reflection and as discussed elsewhere,[5] one realizes that adding 1.0 equiv of a coordinating base such as OH^- *before* the nanoclusters are made cannot, except by accident, yield results identical to those obtained when adding 1.0 equiv of coordinating base *after* the nanoclusters have been made. The reason this is true is that there are many opportunities to influence the nanocluster formation reaction and mechanism during the multistep nanocluster formation reaction (a reaction of at least 300 steps, for example, for an $Ir(0)_{\sim 300}$ nanocluster;[11] again, see elsewhere for more on this point[5]) and when several anionic species are present (e.g., OH^- and $H_2PO_4^-$). This is why Proton Sponge is a good base for nanoclusters formed from metal salts and H_2: it is a strong base but a poorly coordinating ligand.

(16) Sufficient details to make the $\{[Bu_4N][(1,5\text{-COD})Ir{\cdot}HPO_4]\}_n$, 1, complex analytically pure, and thus to repeat any of the work herein, are supplied in the Experimental section. We are continuing work on complex **1**, especially efforts to obtain a single-crystal X-ray diffraction structural analysis, and will report those results elsewhere in due course if they are successful, Özkar, S. Finke, R. G., experiments in progress.

(17) Widegren, J. A.; Aiken, J. D., III; Özkar, S.; Finke, R. G. *Chem. Mater.* **2001**, *12*, 312.

(18) Aiken, J. D., III; Finke, R. G. *J. Am. Chem. Soc.* **1998**, *120*, 9545.

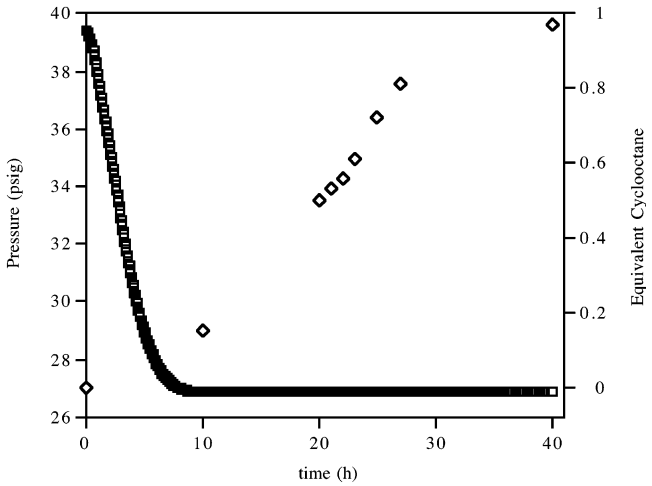

Figure 2. Co-plot of hydrogen pressure (near-solid line formed by overlapping squares; left axis) and cyclooctane production by GLC (individual diamonds; right axis) versus time in the hydrogenation under standard conditions of 1.65 M cyclohexene and concomitant formation of 18 ± 4 Å Ir(0) nanoclusters starting with 1.2 mM $\{[Bu_4N][(1,5\text{-COD})Ir{\cdot}HPO_4]\}_n$ (**1**) in acetone at 22 °C. A 0.5 ± 0.1 h induction period is seen followed by a linear H_2 uptake, $-d[\text{cyclohexene}]/dt = -d[H_2]/dt = 1.0 \pm 0.1$ mmol of H_2/h. Note that almost 40 h is required for complete evolution of 1.0 equiv of cyclooctane and, therefore, for the complete conversion of the $Ir(1,5\text{-COD})^+$ in complex **1** into $Ir(0)_n$ nanoclusters. Hence, a crucial point is that one needs to be able (i) to monitor nanocluster formation in some way, as done herein by the cyclooctane evolution curve, and (ii) to harvest the nanoclusters *after* their complete formation at ca. 40 h in order to measure the properties of the nanoclusters, as opposed to those for an impure, variable mixture of nanoclusters plus the precursor **1**. The use of such a method to follow the nanocluster formation reaction is still an all-too-rare occurrence in the transition-metal nanocluster literature.[1,2]

Quantitative Kinetic Evidence Demonstrating That Ir(0) Nanoclusters Are Formed by Slow, Continuous Nucleation Followed by Autocatalytic Surface Growth. The kinetic curve in Figure 1 also shows the fit to the observed cyclohexene vs time data by the analytic kinetic equation provided elsewhere for the previously elucidated[11a] A → B nucleation (rate constant k_1), and A + B → 2B autocatalytic surface growth (rate constant k_2) mechanism of transition-metal nanocluster formation under H_2. The calculated $k_{1(\text{hydrogenation})}$ and $k_{2(\text{hydrogenation}),\text{corr}}$ values[11a] from this fit are $k_1 = 0.097(1)$ h^{-1} and $k_2 = 0.66(1) \times 10^3$ M^{-1} h^{-1}, respectively; Table 1, entry 1, columns 5 and 6. Note that the k_2 rate constant has been corrected for the mathematically required "stoichiometry" correction factor due to the 1400 equiv of cyclohexene present and because of the pseudoelementary step method used to monitor the reaction (see the Experimental Section, as well as elsewhere,[11a] for further details). The agreement between the observed kinetic data and the analytical fit offers prima facie evidence that the nucleation followed by autocatalytic surface growth mechanism[11a] also applies in this case.

Figure 2 co-plots the GLC-monitored cyclooctane evolution curve beginning with **1**, Scheme 1; note that the reduction of the 1,5-COD ligand in **1** to the easily detected, stable product cyclooctane is a valuable handle built into **1**. Significantly, Figure 2 reveals that less than 20% of the precursor **1** has been converted into active Ir(0) nanoclusters by the time cyclohexene hydrogenation is complete—that is, the ability to monitor the extent of conversion of **1** into nanoclusters is crucial for judging when the nanocluster formation reaction is complete, thereby avoiding artifacts caused by either too-short reaction times leading to their incomplete formation or too-long times leading to their decomposition.

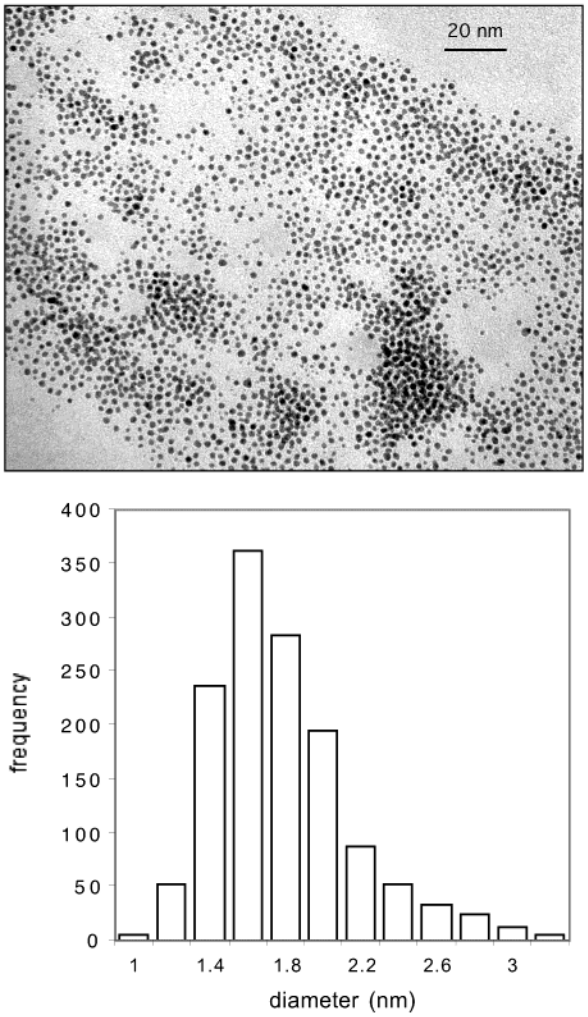

Figure 3. TEM image (430K magnification) and associated particle size histogram of isolated 18 ± 4 Å Ir(0) nanoclusters grown under the standard conditions utilized in these studies (i.e., by the reduction of 1.2 mM **1** in acetone at 22 °C and 40 ± 1 psig of H_2). The particles were isolated after 40 h, redispersed onto a TEM grid, and counted with NIH-Image [1490 non-touching particles; touching particles have necessarily been ignored (see the Experimental Section)].

As the nanocluster formation and concomitant cyclohexene hydrogenation reactions proceed, the clear-yellow solution becomes a darker yellow, then yellow-brown, and finally brown once the iridium precatalyst **1** has been completely converted into active Ir(0) nanoclusters (after ca. 40 h as determined by the GLC-monitored evolution of cyclooctane). The resultant $Ir(0)_n$ nanoclusters can be isolated as a black powder by evaporation under vacuum of the acetone solvent and cyclohexane. The resulting black powder is completely redissolvable, without the formation of detectable bulk Ir(0) metal, in nonaqueous, polar solvents such as acetonitrile or acetone.

Characterization of the Ir(0) Nanoclusters. Figure 3 shows the TEM images and associated particle size histogram of a clear acetonitrile solution of 18 ± 4 Å (±22%) Ir(0) nanoclusters, isolated after the 40 h hydrogen reduction of 1.2 mM **1** in acetone under standard conditions. The apparent tailing toward higher diameters in the histogram in Figure 3, and its implied nanocluster agglomeration, is probably *not* real; instead, it is probably

an artifact of the TEM not being able to detect nanoclusters under 1 nm, a point noted and seen before (compare our Figure 3 with Figure 6 in ref 5a). Other TEMs are available as Supporting Information (Figure S1, a slightly higher magnification than in Figure 3; and Figure S2, TEM of nanoclusters harvested after 13 h of reaction that are, as expected, smaller, 14 ± 4 Å). The main feature of Figure 3 is that HPO_4^{2-} in the precursor **1** allows the formation of obviously well-formed Ir(0) nanoclusters. Note that the actual stabilizer to this point is the conjugate acid, $H_2PO_4^-$, since no base such as Proton Sponge has been added in any of the above experiments.

Electron diffraction was performed on the same sample of Ir(0) nanoclusters cited above. Two electron diffraction images with different exposure times are superimposed to show all the observable rings of the pattern (Figure S3, Supporting Information). The general diffraction pattern matches that of authentic face-centered cubic Au metal powder (examined as a standard fcc system for comparison). By comparing the relative ratios of the ring distances with crystallographic *d* spacing for a face-centered cubic lattice, one can easily recognize the typical ring patterns from the planes [111], [200], [220], [311], and even [222]. This result indicates that, at least for the iridium nanoclusters subjected to the electron beam, the nanoclusters consist of fcc (or, equivalently, ccp) Ir(0) atoms exactly as in bulk Ir(0) metal. There is, however, increasing evidence that nanoclusters made under mild temperature, kinetically controlled conditions, such as those employed herein, may have disordered, at least partially amorphous, structures or surfaces,[19] at least initially and until they are crystallized in the TEM beam.[2a]

Hydrogen Gas-Uptake Stoichiometry during the Formation of Ir(0) Nanoclusters. Given how useful a fully defined reaction stoichiometry has proven in our other nanocluster studies,[2] a hydrogen gas-uptake experiment was performed during the formation of Ir(0) nanoclusters from **1** alone under H_2 (i.e., in the absence of the cyclohexene that is present under a standard conditions synthesis) but in propylene carbonate, a needed change since acetone is slowly hydrogenated under these conditions.[20] Under a H_2 pressure of 154.6 Torr and after an induction period of ca. 0.5 h, a 11.4 mM solution of **1** in propylene carbonate at 22.0 ± 0.2 °C consumes 2.7 ± 0.5 equiv of hydrogen/mol of Ir (Figure S4, Supporting Information) and releases 1.0 ± 0.2 equiv of cyclooctane (by GLC). During this experiment, the original yellow solution changed to the usual dark brown. A control experiment confirmed that the Ir(0) nanoclusters formed in this particular experiment are also active catalysts, hydrogenating cyclohexene, with an induction period of <0.1 h, at a rate of 0.6(1) mmol of H_2/h for the iridium(0) nanoclusters (1.2 mM total Ir concentration). TEM images of Ir(0) nanoclusters in the brown solution after the hydrogen-uptake reaction and associated particle size histograms are available in Figure S5, Supporting Information.

The reaction stoichiometry can be rationalized by Scheme 1, in which 2.5 equiv of H_2 are used to produce 1.0 equiv each of cyclooctane and Ir(0) from the [(1,5-COD)Ir(I)]$^+$ precursor (step I, Scheme 1). The resultant stoichiometry of 2.5 equiv of H_2 per **1** is consistent with the experimental observables of (i) formation of 1 equiv (1.0 ± 0.2) of cyclooctane from the precatalyst **1** (by GLC) and (ii) reduction of the Ir(I) complex to Ir(0) metal (by electron diffraction, Figure S3). Such proof of the balanced reaction stoichiometry for nanocluster formation is still an all-too-rare event.[1,2]

Scavenging the Proton Generated by Hydrogen Reduction of the Precursor Complex 1: Formation of the Monohydrogen Phosphate versus the Dihydrogen Pphosphate Anion. As already noted, 1.0 equiv of H^+ per iridium(I) reduced is generated during the nanocluster synthesis reaction (step I, Scheme 1). The proton will then react with the strongest base present, HPO_4^{2-}, forming $H_2PO_4^-$ (step III, Scheme 1) as the actual stabilizer present in the absence of added base. The more basic, monoprotonated HPO_4^{2-} anion is expected to have better ligating ability toward the electrophilic iridium atoms on the nanocluster surface; hence, base was added in the next set of experiments to scavenge the H^+ byproduct in reaction I, Scheme 1, as step IV therein shows.

Two types of nanocluster synthesis and cyclohexene hydrogenation experiments were performed, separate experiments adding 1.0 and then 2.0 equiv of Proton Sponge into the solution, and then an experiment adding 1 equiv of tetrabutylammonium hydroxide, each at the start[15] of the reaction. These experiments parallel exactly our earlier use of these two bases in analogous experiments testing other anions.[5a,b] The first series of experiments was performed with 1.2 mM **1** in which 1.0 equiv (1.2 mM), and separately 2.0 equiv (2.4 mM), of Proton Sponge were added at the start of two separate nanocluster synthesis reactions. The cyclohexene loss kinetic data for the 1.0 equiv experiment is shown in Figure S6, Supporting Information (since it is not unlike Figure 1); the expected sigmoidal-shaped cyclohexene loss versus time curve is seen for the 1.0 equiv experiment as well as for the 2.0 equiv Proton Sponge experiment (Figure S7, Supporting Information). The important results from these two experiments are that the nanocluster formation kinetic curves and data are, as desired, little changed vs the experiment without added Proton Sponge (cf. entries 2 and 3 with entry 1 in Table 1), and the TEM-determined distributions are also unchanged within experimental error (entries 2 and 3 vs 1 in Table 1, column 8). Significantly, as desired, the solutions remain a homogeneous yellow-brown; the resultant HPO_4^{2-}-and Bu_4N^+-stabilized Ir(0)nanoclusters are isolable and redissolvable without the formation of detectable bulk metal. The nanoclusters show enhanced catalytic lifetimes, for example, the 67 000 and ≤150 000 TTOs for the cases with 2.0 and 1.0 equiv of Proton Sponge, respectively (entries 3 and 2 in comparison to entry 1, Table 1, column 12).

Figure 4 shows the TEM image and associated particle size histogram of isolated 18 ± 4 Å (±22%) Ir(0) nanoclusters formed in the 1.0 equiv of Proton Sponge experiment; the TEM images and the associated particle size histogram for the 2.0 equiv of Proton Sponge experiment are available as Figure S8, Supporting Information. The largely symmetric distributions exhibited in Figure 4 and Figure S8 are noteworthy. Two diffraction images of the same sample used for Figure S6, but with different exposure times, are superimposed to show all the observable rings of the pattern in Figure S9, Supporting Information. The general diffraction pattern indicates ccp, again at least under the crystallizing conditions of the electron beam.[2a]

A control experiment with 1.2 mM **1** but now 1.2 mM Bu_4NOH as the base under otherwise standard conditions was performed; the reaction proceeds slowly with a 4-fold longer induction period of 2.0(2) h vs when no base is added (Table 1, entry 4). After complete hydrogenation of cyclohexene (about 26 h), the solution was still yellow, but closer inspection shows the presence of some black,

(19) De Caro, D.; Bradley, J. S. *New J. Chem.* **1998**, 1267.
(20) Aiken, J. D., III; Finke R. G. *Chem. Mater.* **1999**, *11*, 1035.

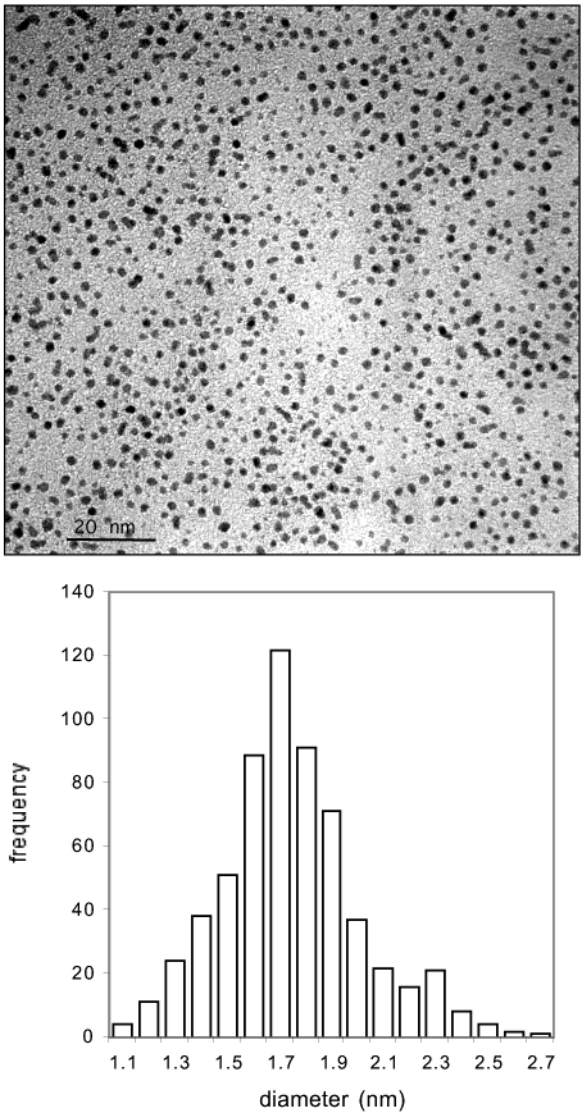

Figure 4. TEM image (580K magnification) and associated particle size histogram (669 nontouching particles counted) of 18 ± 4 Å Ir(0) nanoclusters grown by the reduction of 1.2 mM **1** and 1.2 mM Proton Sponge in acetone under standard conditions for 39.5 h, isolated, and then redissolved in acetone and placed on a TEM grid.

bulk Ir(0) metal precipitate; in addition, the black residue obtained following removal of the volatiles is not completely redispersible in acetone (Table 1, entry 4, column 10). TEM examination of the fraction of the residue that redissolved in acetonitrile revealed smaller Ir(0) nanoclusters with a broader size distribution, 15 ±4 Å (±26%), as well as an abundance of ≥20 Å particles (Table 1, entry 4, column 11, and Figure S10, Supporting Information). In short, the results indicate that, as found with other anion stabilizers,[5a,b] weakly coordinating but strong bases, such as Proton Sponge, as the added H^+ scavenger yield nanoclusters with better properties than does Bu_4NOH.

Changing the Concentration of HPO_4^{2-}: Nanocluster Size Control, Evidence for the Reduction of Free $[(1,5\text{-COD})Ir(acetone)_2]^+$ in the Nanocluster Formation Reaction, and Evidence for HPO_4^{2-} Coordination to the Ir(0) Nanocluster Surface. On the basis of our earlier work,[11] our expectation was that, by adding[21] HPO_4^{2-} to nanocluster formation reactions (e.g., starting with the precursor complex **1**), we would see an increase in induction period, a smaller k_2/k_1 ratio, and the concomitant formation of smaller nanoclusters—that is, that some level of size control would be attainable by controlling the HPO_4^{2-} concentration. As entries 5 and 6 in Table 1 in comparison to entry 1 show, just the expected, albeit modest, effects are seen for the moderate amounts of $[Bu_4N]_2HPO_4$ added to the solution: the induction period increases from 0.5 to 6.0 and 12 h (for 0, 1, and 4 equiv of $[Bu_4N]_2HPO_4$ added to the solution over and above the 1 equiv of HPO_4^{2-} present in **1**). In addition, the average size of the resultant Ir(0) nanoclusters decreases from 18 to 16 to 13 Å with 0, 1, and 4 equiv of added $[Bu_4N]_2HPO_4$ (Table 1, entries 1, 5, and 6, column 8; TEM images are available as Figure S11, Supporting Information; note that the error bars are ±4 Å). Unfortunately, we were not able to reliably measure the more sensitive k_2/k_1 predictor of initial nanocluster size[5,11b] due to the long induction periods; however, since it is known that $1/k_1 \propto t_{ind}$, and t_{ind} is increasing significantly with added $[Bu_4N]_2HPO_4$, it is highly likely that k_2/k_1 is decreasing with 1 and 4 equiv of added $[Bu_4N]_2HPO_4$ as expected for the formation of smaller nanoclusters.[11b] Moreover, these results parallel those for the $P_2W_{15}Nb_3O_{62}^{9-}$ anion where an extra ~8 equiv of polyoxoanion give 15 ± 4 Å, vs the normal 21 ± 4 Å, Ir(0) nanoclusters.[11a,b]

This significant increase in the induction period with increasing amounts of added $[Bu_4N]_2HPO_4$ is excellent evidence for the small equilibrium constant (≪1) of a dissociative preequilibrium, eq 1, being part of the nucleation steps, results exactly analogous to the similar dissociative equilibrium detected in the same way for the $[(1,5\text{-COD})Ir{\cdot}P_2W_{15}Nb_3O_{62}]^{8-}$ precursor.[11a] In other words, the inverse HPO_4^{2-} dependence is excellent evidence that dissociated, freely diffusing, cationic, and thus more easily reduced $[(1,5\text{-COD})Ir(acetone)_2]^+$ is, as suggested before,[11] the true A species of the A + B → 2B autocatalytic surface growth step in nanocluster formation:

$$\frac{1}{n}\{[(COD)Ir{\cdot}HPO_4]^-\}_n + 2\text{acetone} \leftrightarrows [(1,5\text{-COD})Ir(acetone)_2]^+ + HPO_4^{2-} \quad (1)$$

Finally, the hydrogenation rate decreases by an order of magnitude with added $[Bu_4N]_2HPO_4$: $-d[H_2]/dt = 1.0$, 0.2, and 0.1 mmol of H_2/h for 0, 1, and 4 equiv of additional HPO_4^{2-} added to the solution (Table 1, entries 1, 5, and 6). This result is readily explained as well:[11a] increasing the concentration of hydrogen phosphate results in a higher coverage of the iridium(0) nanocluster surface, thereby inhibiting the catalytic reactions of the Ir(0) active sites—indeed, this is prima facie evidence that the HPO_4^{2-} is binding to the Ir(0) nanocluster's electrophilic surface.

Controls Generating the Ir(0) Nanoclusters via the in Situ Precursors Route with $[(1,5\text{-COD})Ir(NCCH_3)_2]BF_4$ plus $[Bu_4N]_2HPO_4$, plus Controls with Added Proton Sponge or Bu_4NOH. As noted in the Introduction, there are basically two general ways to generate nanoclusters by the reduction of metal salts under H_2: (i) the slower, more demanding use of chemically well-defined precursor complexes such as $\{[Bu_4N][(1,5\text{-COD})Ir{\cdot}HPO_4]\}_n$, **1**, as employed to this point and as we

(21) Note here that isolable, solid-state stable $[Bu_4N]_2HPO_4$ is unknown in the literature, presumably because of its instability due to Hoffmann elimination to give butene, Bu_3N, and the diprotonated $H_2PO_4^-$. Hence, the $[Bu_4N]_2HPO_4$ used throughout this work was necessarily generated in situ from commercially available dihydrogen phosphate, $[Bu_4N]H_2PO_4$, plus 1.0 equiv of Bu_4NOH, with the resultant 1 equiv of H_2O being removed by use of molecular sieves as detailed in the Experimental Section.

have successfully emphasized before in our $P_2W_{15}Nb_3O_{62}^{9-}$ polyoxoanion-stabilized nanoclusters;[11,12,17,18,20,22] or (ii) the much faster, more versatile, in situ mixing of the metal precursor and anionic stabilizer, in the present case [(1,5-COD)Ir(solvent)$_2$]BF_4 plus $[Bu_4N]_2HPO_4$. The main advantage of the in situ route is its ease and speed of adaptation to new anionic or other stabilizers. The main disadvantages of the in situ route, even with careful weighing and transfer of the precursors as we have employed herein, are (a) the loss of precise control over the exact amount of free [(1,5-COD)Ir(solvent)$_2$]$^+$ (and its aforementioned dramatic effects on the induction period and reduced kinetic control over the nanocluster synthesis[11a]), (b) issues related to any slow ligand substitution rates at the reaction conditions employed (although this is not expected to be a problem for the 16-electron, substitutionally labile [(1,5-COD)Ir(solvent)$_2$]$^+$ complex at the 22 °C conditions employed), and (c) the fact that the [(1,5-COD)Ir(solvent)$_2$]BF_4 + $[Bu_4N]_2HPO_4$ route gives not only **1** but also 1 equiv of Bu_4NBF_4 + $2CH_3CN$ as byproducts and in comparison to experiments starting with isolated **1**. There is also (d) the fact that any problems with the in situ route would tend to lead to the loss of the ±15% reproducibility we have come to enjoy via the precursor complex route if one controls the other key variables,[11] notably the source of the acetone solvent, its age,[13] and its water content.[11,12]

As part of our work generating the anion efficacy series,[5a,b] key controls were done up front to show that, at least for the $P_2W_{15}Nb_3O_{62}^{9-}$ polyoxoanion, results generally equivalent within experimental error were obtained by use of either the preformed complex or in situ routes.[5a,23] The needed experiments were performed starting with [(1,5-COD)Ir(NCCH$_3$)$_2$]BF_4 plus just $[Bu_4N]_2HPO_4$ to start, then in separate experiments with 1.0 equiv of Proton Sponge or 1.0 equiv of $Bu_4N^+OH^-$ added (entries 7, 8, and 9 in Table 1). In comparison to the preformed complex, **1**, without base (compare entries 7 and 1, Table 1), the in situ route is much less effective at a kinetically controlled synthesis of completely soluble and totally redissolvable nanoclusters (note the short induction period, bulk metal precipitate, and only partially redissolvable product produced by the in situ route, entry 7). Adding 1 equiv of Proton Sponge at the start of the reaction dramatically improves the in situ synthesis (entry 8 vs entry 7) and yields results that are comparable, but not identical, to those for the analogous preformed complex plus Proton Sponge (entry 8 vs entry 2; the Proton Sponge kinetic curve and TEM are provided as Figures S12 and S13, Supporting Information). We checked to be sure that the age of the Burdick and Jackson acetone[13] was not influencing these results: we found that the results either with the preformed complex **1** or via the in situ experiments were still within experimental error. The addition of 1 equiv of $Bu_4N^+OH^-$ to the in situ route yields reasonable nanoclusters, ones that are even a bit better in some respects than those made via the preformed complex route plus $Bu_4N^+OH^-$ (entry 9 in comparison to entry 4 in Table 1; the kinetic curve and TEM for the data in entry 9 are provided as Figures S14 and S15, Supporting Information). However, the catalytic activity and lifetime are a bit lower in comparison to the preformed complex route with 1 equiv of $Bu_4N^+OH^-$. That these effects are mostly a OH^- effect is suggested by the fact that addition of a second equivalent of $Bu_4N^+OH^-$ (i.e., 2.0 equiv total) yields bulk metal, results that mimic those seen previously for OH^- plus [(1,5-COD)Ir(NCCH$_3$)$_2$]BF_4.[5b]

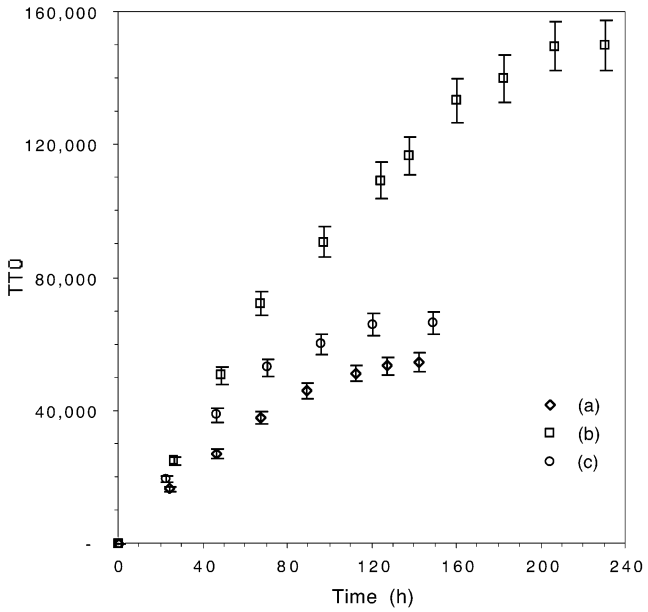

Figure 5. Variations in the total turnover number (TTO) as a function of time in the cyclohexene hydrogenation in acetone at 22 °C starting with (a) (diamonds, bottom curve) 1.44 μmol $\{[Bu_4N][(1,5\text{-COD})Ir\cdot HPO_4]\}_n$ (**1**) (computed for $n = 2$); (b) (squares, top curve) 0.72 μmol of **1** plus 0.72 μmol (1 equiv) of Proton Sponge added at the start of the reaction; and (c) (circles, middle curve) 0.72 μmol of **1** plus 1.44 μmol (2 equiv) of Proton Sponge added at the start of the reaction.

The bottom line of these experiments is that, for HPO_4^{2-} (as well as for $P_3O_9^{3-}$ as detailed above), the exact details of the synthesis matter: the preformed complex yields the best nanocluster formation and stabilization results, all data considered. Another take-home message consistent with this as well as our earlier work[5,11,12] is that tight complexation of (1,5-COD)Ir$^+$ by the stabilizing anions yields kinetically slower, more highly controlled nucleation, leading to better formed, less agglomerated nanoclusters.[24]

A Closer Look at the Catalytic Lifetime and the Postcatalysis TEM Images of $[Bu_4N]_2HPO_4$- and $[Bu_4N]H_2PO_4$-Stabilized Ir(0) Nanoclusters without, and with, Added Proton Sponge. The TTOs of cyclohexene hydrogenation in solution by soluble nanoclusters provide a fairly rigorous test of nanocluster stabilization, one that also assays whether the anion allows sufficient unencumbered surface area for high catalytic rates (and thus larger TTO values). For this reason the TTO data for three of the most important TTO experiments are shown in Figure 5: starting with **1** alone, with 1.0 equiv, and with 2.0 equiv of added Proton Sponge in acetone at 22 °C and 40 psig of H_2 pressure.

(22) Aiken, J. D., III; Finke, R. G. *J. Am. Chem. Soc.* **1999**, *121*, 8803.

(23) In the case of less Brønsted basic $P_3O_9^{3-}$ ligand, we did notice that starting with the preformed complex (1,5-COD)Ir·$P_3O_9^{2-}$—with its somewhat unusual 5 coordinate, 18 electron Ir(I)—did provide very high kinetic control into initially soluble, albeit polydisperse, nanoclusters. These materials did begin to precipitate from solution within a day, however.[5b] In short, both synthetic routes using $P_3O_9^{3-}$ yielded considerable bulk metal and led to a similar anion efficacy ranking for the $P_3O_9^{3-}$ ligand.[5b] Nevertheless, it is important to experimentally test the preformed complex and in situ routes when one can, as the results cited above for (1,5-COD)Ir·$P_3O_9^{2-}$, and given in the text for HPO_4^{2-}, demonstrate.

(24) A control experiment with the diprotonated $[Bu_4N]H_2PO_4$ plus [(1,5-COD)Ir(NCCH$_3$)$_2$]BF_4 in an in situ synthesis was carried out; note that the conjugate acid H_3PO_4 is the resultant stabilizer here, so that relatively little stabilization is expected. Little kinetic control in the synthesis and only insoluble product was observed (entry 11, Table 1). No discernible improvement was seen when 1 equiv of Proton Sponge was added (entry 12, Table 1).

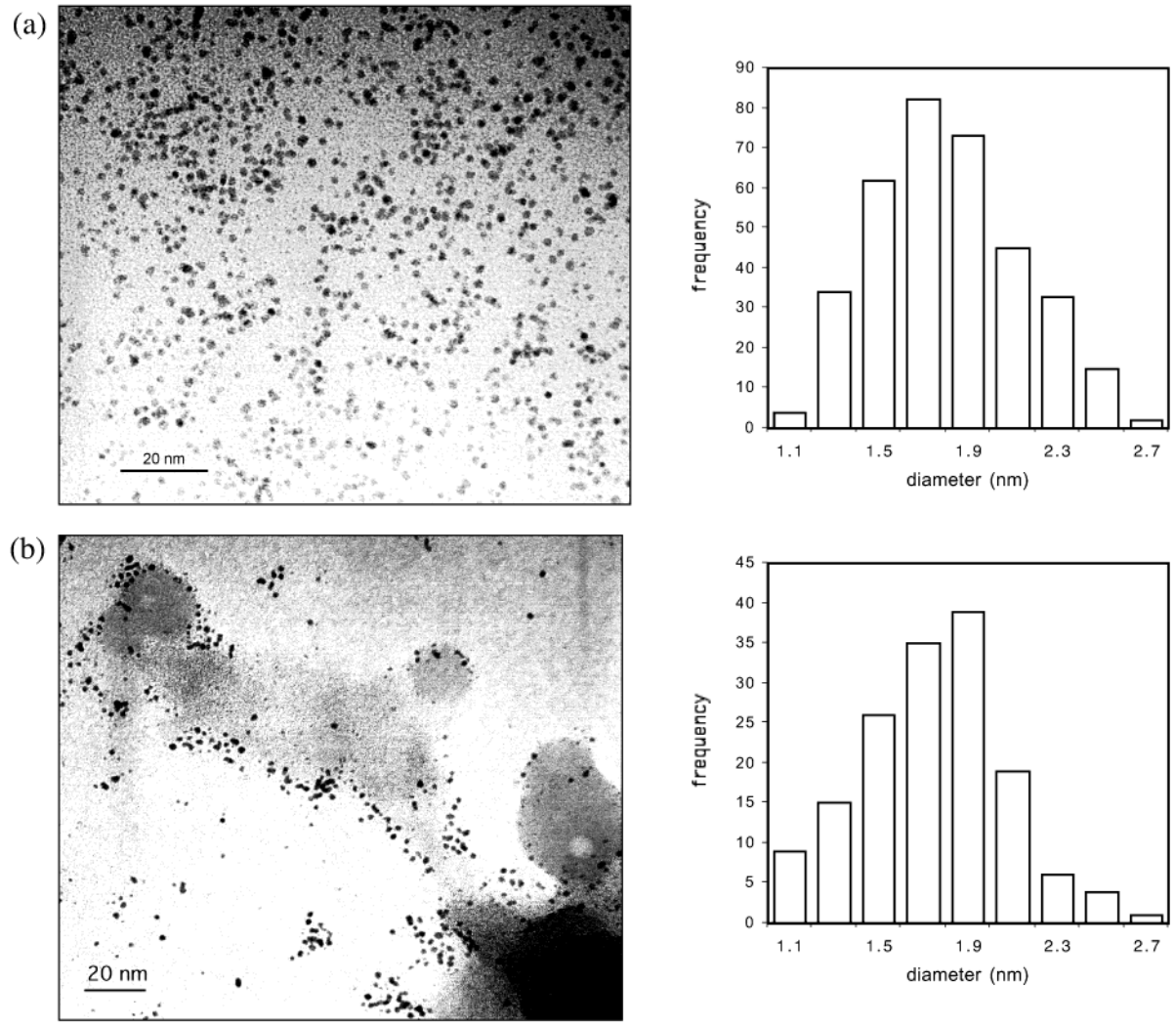

Figure 6. TEM images (430K magnification) and associated particle size histograms: (a) Ir(0) nanoclusters isolated after completion of 2800 TTOs of cyclohexene hydrogenation at 22 °C and 40 ± 1 psig of H_2. The nanoclusters were first grown by the reduction of 1.2 mM **1** in acetone under standard conditions and then isolated and redissolved in acetone along with 1.65 M cyclohexene for a second hydrogenation (of 1400 additional TTOs). Next, they were reisolated from the catalytic reaction solution at the end of the reaction, redissolved in acetonitrile, and then placed on a TEM grid for the TEM image shown. This top TEM and associated histogram shows 18 ± 5 Å particles (n = 525 nontouching particles counted). (b) Ir(0) nanoclusters isolated and then redissolved in acetonitrile and placed on a TEM grid after a lifetime experiment of 55 000 TTOs at 22 °C and 40 ± 1 psig of H_2. The TEM and associated histogram shows bulk metal in addition to still present, 18 ± 5 Å particles (n = 154 nontouching particles counted).

Starting with 1.44 μmol **1**, dihydrogenphosphate-stabilized Ir(0) nanoclusters give 55 000 TTOs over 6 days before deactivation (Figure 5; dihydrogen phosphate-stabilized due to the unscavenged proton released in the nanocluster formation reaction, vide supra). Clearly the 1 equiv of Proton Sponge is best in terms of TTOs, 150 000 over 9 days before deactivation; increasing the Proton Sponge to 2 equiv hurts the TTOs, decreasing it to 67 000 over 5 days before deactivation. The TEM after the 67 000 TTOs in the presence of 2 equiv of Proton Sponge provides clear evidence for nanocluster agglomeration as a deactivation pathway (Figure S16, Supporting Information).

Figure 6 shows the TEM images of the iridium(0) nanoclusters, formed from the reduction of **1** under standard conditions hydrogenation, (a) after they are isolated, redissolved, and undergo one cycle of catalytic activity (ca. 2800 turnovers) and (b) after their TTOs experiments (they are isolated and then redissolved in acetonitrile for the TEM shown in Figure 6b). The TEM image in Figure 6b shows agglomeration of nanoclusters into bulk metal after 6 days and 55 000 TTOs (see the right-hand bottom of Figure 6b), as expected on the basis of visual observation of bulk metal precipitation at the end of lifetime experiment. However, there are still some Ir(0) nanoclusters of the same size as the ones seen in Figure 6a. The caveat here is that touching nanoclusters are avoided in the NIH image counting of them, as detailed in the Experimental Section, which in turn biases the analysis toward the smaller (i.e., nonagglomerated) nanoclusters. As a check, the TEMs were obtained after the 53 000 and 17 800 TTOs for the in situ route experiments with Proton Sponge and $Bu_4N^+OH^-$ (entries 8 and 9, Table 1; Figure S17, Supporting Information). Overall, the results show that agglomeration accompanies deactivation.

The TEM images and associated histograms of the 150 000 turnovers experiment with 1 equiv of Proton Sponge (Figure 7), after only 1400 TTOs and then after the 150 000 TTOs, again show that there has been aggregation. Some Ir(0) nanoclusters of ca. the original size, 19 ± 5 Å, do still exist, although those nanoclusters must have suffered some surface-deactivation process since the activity is now near zero. Hence, there is likely at least some contribution from bulk metal in the 150 000

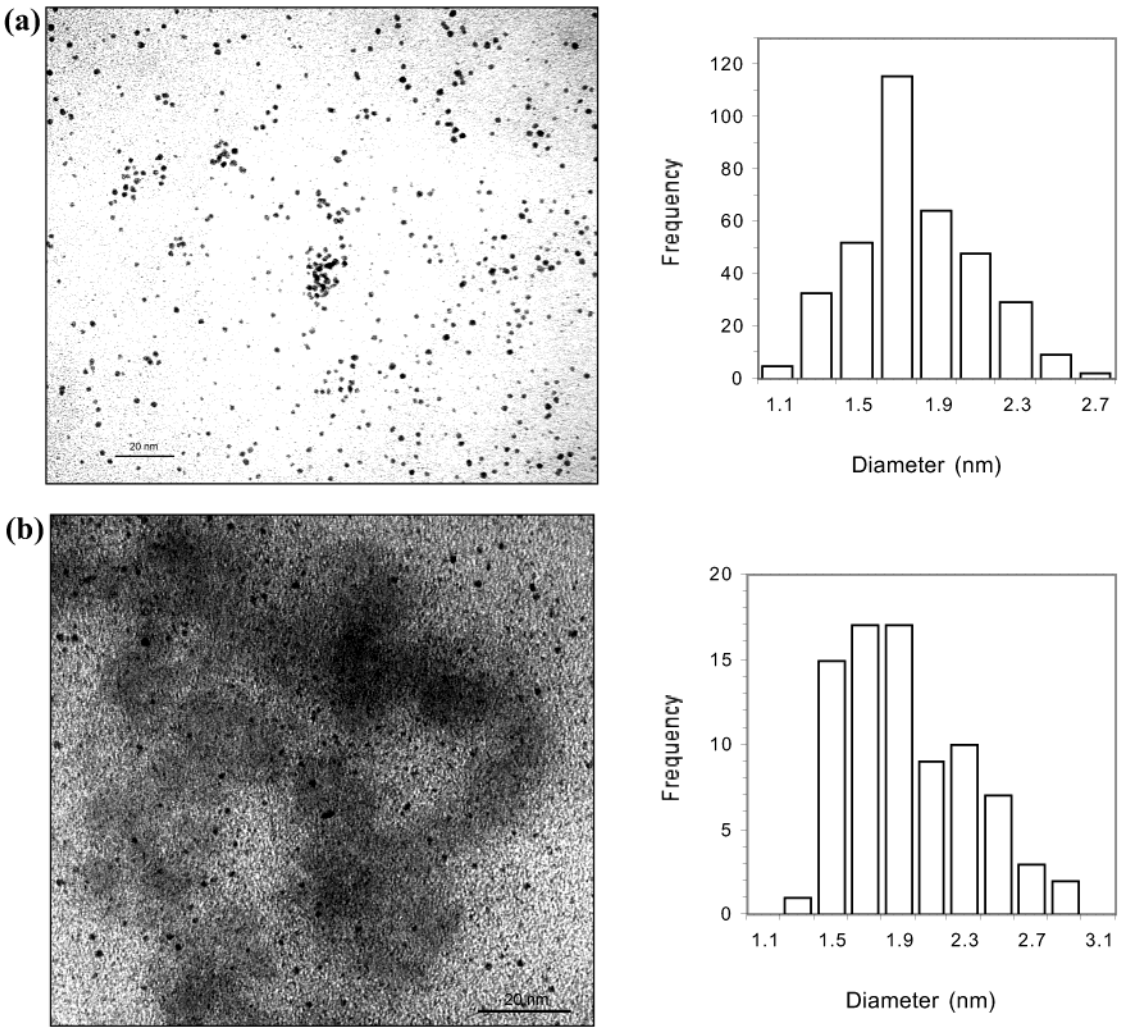

Figure 7. TEM images (430K magnification) and associated particle size histograms: (a) Ir(0) nanoclusters were first grown by the reduction of 1.2 mM **1** in acetone plus 1.2 mM Proton Sponge but otherwise were handled exactly as described for Figure 6a. This top TEM and associated histogram shows 18 ± 4 Å (n = 358 nontouching particles counted). (b) Ir(0) nanoclusters formed from 0.72 μmol of **1** and 0.72 μmol (1 equiv) of Proton Sponge during a lifetime experiment of 150 000 TTOs at 22 °C and 40 ± 1 psig of H_2. The nanoclusters were isolated and then redissolved in acetonitrile and placed on a TEM grid after completion of the TTO experiment. The bottom TEM and associated histogram shows agglomerated nanoclusters plus 19 ± 5 Å particles (only n = 81 nontouching particles could be counted).

TTOs, a number we therefore regard as an upper limit to the true TTOs exhibited by the Ir(0) nanoclusters from **1** plus 1 equiv of Proton Sponge.

The ≤150,000 TTO value is, nevertheless, almost surely a record[25] for Ir(0) nanoclusters, eclipsing the recently set, directly comparable record of 68 000 for Ir(0) nanoclusters[5] beginning with $[(1,5\text{-COD})Ir{\cdot}P_2W_{15}Nb_3O_{62}]^{8-}$ plus 1 equiv of Proton Sponge. The ≤150 000 TTOs are even sizable in comparison to the current absolute record of 190 000 TTOs for polyoxoanion-stabilized Rh(0) (and thus more catalytically active) nanoclusters in solution.[22] An important observation here is that Proton Sponge is an effective proton-scavenging additive from the standpoint of catalytic activity.

A Comparison of the Most Effective Anionic Stabilizers for Ir(0) Nanoclusters. Table 2 summarizes the data for the most effective anion stabilizers presently known[5] for Ir(0) nanoclusters in the nonprotic organic solvent acetone and with Bu_4N^+ as the accompanying cationic stabilizer. A perusal of Table 2 indicates that the polyoxoanions $P_2W_{15}Nb_3O_{62}^{9-}$, as well as its associated Nb−O−Nb bridged anhydride $[(P_2W_{15}Nb_3O_{61})_2O]^{16-}$, are the best anions (the present "gold standards")[5a,b] according to the five criteria, primarily due to their 2 orders of magnitude larger value for the crucial k_2/k_1 ratio (and its associated higher level of kinetic control in the nanocluster synthesis) but also due to small advantages in narrower nanocluster dispersities (14% for the best case of the $[(P_2W_{15}Nb_3O_{61})_2O]^{16-}$ polyoxoanion vs 22% for HPO_4^{2-}) and catalytic rates (higher by a factor of ∼2). The HPO_4^{2-} anion does have the edge in the number of TTOs (the ≤150 000 value), however.

In comparison to the commonly used citrate^{3-} anion, HPO_4^{2-} holds the edge in catalytic activity and TTOs but is ca. 18-fold less effective in its kinetic control as measured by the k_2/k_1 ratio (compare entries 3 and 5). Overall, the previously unrecognized HPO_4^{2-} performs equivalently to the widely employed citrate^{3-}, with a ranking HPO_4^{2-} ∼ citrate^{3-} in the anion series. This is a significant finding. The HPO_4^{2-} ∼ citrate^{3-} finding is also valuable in that it verifies the first prediction of the lattice size-matching

(25) Besides being a record for Ir(0) nanoclusters, values approaching 150 000 TTOs of cyclohexene hydrogenation are sizable even in comparison to Exxon's 80% dispersed Ir(0)/η-Al_2O_3 catalyst, which dies after 20 000 TTOs of cyclohexene hydrogenation in acetone under very similar conditions.[12b] Even commercial 7.9% dispersed Ir(0)/γ-Al_2O_3 gives a value that is only ca. 3 times larger, 410 000 TTOs.[12b]

Table 2. Key Data[a] for Comparing the Most Effective Ir(0)$_n$ Nanocluster Stabilizing Anions According to the Five Criteria

entry	stabilizing anion	(i) k_2/k_1 ratio	(ii) nanocluster dispersity (Å)	(iii) fully redissolvable in acetone?	(iv) catalytic activity after redispersion[b] (mmol of H_2/h)	(v) TTOs of cyclohexene hydrogenation
1	$P_2W_{15}Nb_3O_{62}^{9-}$	4.4×10^5	21 ± 4	yes	2.2	68 000
2	$[(P_2W_{15}Nb_3O_{61})_2O]^{16-}$	1.9×10^5	22 ± 3	yes	1.9	40 000
3	HPO_4^{2-} (i.e., when 1 equiv of Proton Sponge is added)	7.2×10^3	18 ± 4	yes	0.8	[150 000][c]
4	$H_2PO_4^-$ (i.e., when no base is added)	6.8×10^3	18 ± 4	yes	1.0	55 000
5	citrate^{3-} (i.e., when 1 equiv of Proton Sponge is added)	1.3×10^5	18 ± 4	yes	0.4	7600
6	citrate^{3-}	$[0.50 \times 10^5]$[d]	23 ± 5	partial	0.4	[43 000][c]

[a] Data for the $P_2W_{15}Nb_3O_{62}^{9-}$ and $[(P_2W_{15}Nb_3O_{61})_2O]^{16-}$ polyoxoanions, and for citrate, are taken from our earlier work.[5a,b] [b] Catalytic activity is for cyclohexene hydrogenation, under standard conditions, of the isolated Ir(0) nanoclusters redispersed in acetone. [c] The brackets indicate that this is an upper limit due to the formation of bulk metal. [d] A different mechanism exists here with, apparently, a second nucleation mechanism when citrate^{3-} is present as discussed in the main text and elsewhere.[5a] Hence, this k_2/k_1 value is not directly comparable to the others in this table.

model, namely, that HPO_4^{2-} would be a good stabilizer for Ir(0)$_n$ and other, selected transition-metal nanoclusters.[5c]

Two other important conclusions are apparent from the data in Table 2. Perusal of the k_2/k_1 and nanocluster dispersity data for citrate^{3-} by itself in entry 6 in Table 2, vs that in entries 1−5, reveals that the data in entry 6 fall out of the pattern seen for the rest of the k_2/k_1 and nanocluster size dispersity data in Table 2 and tabulated before[5a,b] in that a higher k_2/k_1 value for entry 6 does *not* correlate with a narrower size distribution. The reason is almost surely the citrate^{3-}-dependent nucleation pathway for citrate (i.e., in addition to the usual, slow, continuous nucleation pathway for citrate[11a]), first noted by Turkevich and co-workers[26] and then supported by kinetic data in our recent work.[5a] In other words, only in the presence of Proton Sponge or similar bases does the ranking HPO_4^{2-} ∼ citrate^{3-} hold; on its own, due to the presence of an additional nucleation pathway and the loss of kinetic control, the ranking HPO_4^{2-} > citrate^{3-} would be more appropriate.

A second conclusion is one we have already come to[5a,b] but merits reemphasis: when any bulk metal is present, the TTO criterion in Tables 1 and 2 becomes much less reliable. The anomalously high TTOs in entries 3 and 6 in Table 2 fall into this category.

Summary and Conclusions

The present study addresses the hypothesis that HPO_4^{2-} is an effective, simple, readily available yet previously unrecognized anion for the stabilization of transition-metal(0) nanoclusters.[5c] The following are the main findings from this work:

(1) Hydrogen phosphate was shown to be an effective anion for the formation and then stabilization of Ir(0) transition-metal nanoclusters in acetone and with Bu_4N^+ countercations, ranking alongside citrate^{3-} in the anion efficacy series. Hydrogen phosphate is a good stabilizer since it is dianionic and therefore presents a greater Coulombic barrier to nanocluster agglomeration by DLVO theory[6]; it is fairly basic (i.e., is a good σ-donor); it is a tridentate binding, chelating oxygen-donor ligand; and its O−O bond distances can be a good match to the surface Ir−Ir distances, all as the lattice size-matching model suggests is optimum.[5c] Hydrogen phosphate also possesses a number of the same advantages that the $P_2W_{15}Nb_3O_{62}^{9-}$ polyoxoanion has, namely, HPO_4^{2-} is thermally robust and highly oxidation-resistant and it contains a valuable ^{31}P NMR handle. Hydrogen phosphate has the additional advantages of being cheap, more readily available, and much more resistant to reduction in comparison to the otherwise premier anionic tridentate oxoanion stabilizer,[5] the $P_2W_{15}Nb_3O_{62}^{9-}$ polyoxoanion.

(2) With the addition of HPO_4^{2-}, the now expanded "anion series" [5] becomes the following: $P_2W_{15}Nb_3O_{62}^{9-}$ ∼ $[(P_2W_{15}Nb_3O_{61})_2O]^{16-}$ ∼ $([P_2W_{15}(TiOH)_3O$∼$59]^{9-})_n$ ($n = 1$, 2) ∼ $SiW_9Nb_3O_{40}^{7-}$ > HPO_4^{2-} ∼ $C_6H_5O_7^{3-}$ > > $[-CH_2CH(CO_2^-)-]_n^{n-}$ ∼ OAc^- ∼ $P_3O_9^{3-}$ ∼Cl^- ∼ OH^-. The essence of this series is polyoxoanions > HPO_4^{2-} ∼ $C_6H_5O_7^{3-}$ > other commonly used anions.

(3) The HPO_4^{2-} system was shown to exhibit the key observables characteristic of the slow, continuous nucleation and then fast autocatalytic surface growth mechanism first detailed elsewhere,[11] A → B (rate constant k_1) followed by A + B → 2B (rate constant k_2), a nanocluster formation mechanism now known to be more general for transition-metal nanocluster formation under H_2.[2,5] Proof of the balanced reaction stoichiometry for formation of the nanoclusters was provided, including a cyclooctane evolution curve that tells when the nanoclusters are completely formed and thus when it is best to harvest them.

(4) Proton Sponge was shown to be a preferred scavenger relative to $Bu_4N^+OH^-$ for the H^+ byproduct for both HPO_4^{2-} and citrate^{3-} (recall entries 5 vs 6 in Table 2), results that confirm earlier, analogous findings.[5b]

(5) Nanocluster size control over a modest 13−18 Å range was demonstrated simply by changing the HPO_4^{2-} concentration and, therefore, the resultant k_2/k_1 ratio.[5a,11a] Larger size range differences should be possible by using larger concentrations of HPO_4^{2-}, although slow nanocluster formation rates will limit the practical HPO_4^{2-} concentration range one can employ.

(6) The preformed precursor route, employing the previously unknown $\{[Bu_4N][(1,5\text{-COD})Ir{\cdot}HPO_4]\}_n$, **1**, was shown to yield superior nanoclusters over the in situ route for the case of $H_2PO_4^{2-}$. The results suggest that both the preformed complex and in situ routes to nanoclusters merit examination whenever possible. Although the present nanoclusters were not isolated, in recent work we have worked out the preferred solvent, isolation procedures, and other details necessary to isolate and place in a bottle 1 g amounts of nanoclusters that retain ∼65% of their "as formed" catalytic activity.[27]

(7) The catalytic lifetime studies showed that Proton Sponge has a positive effect on the catalytic lifetime, and the postcatalysis TEM studies showed that nanocluster

(26) (a) Turkevich, J.; Stevenson, P. C.; Hillier, J. *Discuss Faraday Soc.* **1951**, *11*, 55. (b) Turkevich, J.; Kim G. *Science* **1970**, *169*, 873.

(27) Hornstein, B. J.; Finke, R. G. *Chem. Mater.* **2003**, *15*, 899.

agglomeration is common following extended catalytic lifetimes even for these relatively highly stabilized nanoclusters.

(8) Finally, and as first noted elsewhere,[28] the results provide molecular-level insight to guide the molecularly ill-understood area of phosphating of metal surfaces[7f−k] to achieve corrosion resistance, electrical resistance, or bonding to organic coatings such as rubber. One insight, for example, is that HPO_4^{2-} should prefer the metals where there is a good lattice size match, especially Co, Ni, and Cu but also Fe, Ru, Rh Ir, Pd, Re, Os, and Pt.[29] In addition, the findings herein foretell the use of phosphate, plus custom-made derivatives of deprotonated alkyl- and arylphosphonic acids, RPO_3^{2-}, in the areas of metal surface treatment for enhanced material properties.[7g]

Overall, it is clear that HPO_4^{2-} is a previously unrecognized, effective stabilizer for at least Ir(0) nanoclusters. Moreover, lattice size-matching considerations[5c] suggest that HPO_4^{2-} merits consideration anytime M(0) nanoclusters of Fe, Co, Ni, Ru, Rh, Ir, Pd, Re, Os, or Pt are planned.[29]

Experimental Section

A summary of the main experimental procedures is given below. More detailed experimental procedures are provided in the Supporting Information.

Materials. All commercially obtained compounds were used as received unless indicated otherwise: acetone was purchased from Burdick & Jackson (water content <0.2%) and was purged with argon and transferred into a nitrogen atmosphere drybox before use. It is known that the source, age,[13] and H_2O content of the acetone all matter in achieving reproducible nanocluster syntheses.[11a,12b] Cyclohexene (Aldrich, 99%) was purified by distillation over sodium under argon and stored in the drybox. Aqueous Bu_4NOH solutions (40% in water, Aldrich, freshly opened) were titrated separately with 0.1 M HCl to methyl red and phenolphthalein end points (i.e., for both amine and total base content) immediately prior to use. Solutions of either Proton Sponge (Aldrich) or Bu_4NOH in acetone were made fresh and should not be stored for long periods of time due to aldol condensation reactions and different, enhanced catalytic rates from older solutions.[13] $AgBF_4$ (Aldrich) was purified by extraction with diethyl ether followed by evaporation of the extract under vacuum to give a white powder. Deuterated NMR solvents CD_3CN and CD_2Cl_2 (Cambridge Isotope Laboratories) were received in 1 mL glass ampules, which were transferred into the drybox for NMR sample preparations done there. The iridium solvate complex, $[(1,5\text{-COD})Ir(NCCH_3)_2]BF_4$, was prepared as yellow crystals according to the procedure given in the literature for the corresponding hexafluorophosphate salt;[30b] the product was identified by ^1H and ^{13}C spectroscopy in comparison with the literature spectral data.[30b]

Analytical Procedures. Unless otherwise reported, all reaction solutions were prepared under oxygen- and moisture-free conditions in a Vacuum Atmospheres nitrogen drybox (<1 ppm O_2 as continuously monitored by a Vacuum Atmospheres O_2-level monitor).

The hydrogen gas-uptake stoichiometry experiment was performed in the general manner previously described.[20] The uptake apparatus was described in detail previously (see Figure K of the Supporting Information in ref 20).

Gas−liquid chromatography (GLC) of the cyclooctane hydrogenation product was performed on a Hewlett-Packard 5890 Series II GC with a FID detector equipped with a 30 m (0.25 mm i.d., 25 μm film) Dowex DB-1 column coupled to a Hewlett-Packard 3395 integrator. Parameters were as follows: initial temperature, 50 °C; initial time, 3 min; ramp, 10 °C/min; final temperature, 160 °C; final time, 16 min; injector port temperature, 180 °C; detector temperature, 200 °C; injection volume, 4 μL.

High-resolution solution NMR spectra were taken on a Varian INOVA-300 instrument (^1H, 300.115 MHz; ^{13}C, 75.472 MHz; and ^{31}P, 121.489 MHz). IR spectra were taken on a Nicolet 5PC FTIR spectrometer. Elemental analyses were done by Atlantic Microlab.

Transmission Electron Microscopy and Electron Diffraction Studies. TEM analyses were performed as before[5,11,12] at the University of Oregon with the expert assistance of Dr. Eric Schabtach, using the sample preparation procedure and using a Philips CM-12 TEM with a 70 μm lens operating at 100 kV and with a 2.0 Å point-to-point resolution, as described in detail previously.[12a] Typically, TEM pictures of each sample were taken at three different magnifications (100K, 200K, and 430K) in order to obtain information about the sample in general (100K), plus a closer visualization of the clusters (430K). A number of control experiments were done previously, which provided good evidence that the results—at least for the present $Ir(0)_n$ nanoclusters—are representative of the sample, save any crystallization that occurs in the TEM beam [e.g., controls showing that varying the sample spraying method (in air or under N_2) or depositing the sample as a drop and letting it dry did not change the results; controls showing that changing the beam voltage from 40 to 100 kV, or changing the exposure time (seconds vs minutes), did not change the images; other controls have been done as well].[12a] Electron diffraction patterns were taken on the same instrument with a 530 or 770 mm camera length with the selected area generally containing hundreds of Ir(0) nanoparticles. Samples for both TEM and electron diffraction studies were prepared by dispersing the Ir(0) nanocluster solution onto a copper grid covered with an amorphous carbon thin film.

Sample Preparation for TEM and Electron Diffraction. The solutions used for the TEM and electron diffraction experiments were the exact same ones described in the following sections on standard conditions and catalytic lifetime experiments. However, at the end of a given run (i.e., at a minimum time required for the complete formation of nanoclusters in the standard conditions hydrogenation and at the end of catalytic lifetime experiments), the Fischer−Porter (F−P) bottle was detached from the hydrogenation line via its quick-connects and brought back into the drybox, and its acetone solution was transferred with a disposable polyethylene pipet into a clean, 5 mL screw-capped glass vial. (In cases where bulk metal precipitation is observed, samples were harvested just before agglomeration starts. In catalytic runs, TEM samples were taken at the end of the catalytic lifetime experiment.) The solution was then dried in a vacuum and the glass vial was sealed and brought out of the drybox. The dry nanocluster samples in screw-capped glass vials were sent as solids to the University of Oregon for TEM investigation. There, 1 mL of acetonitrile was added, in air, just before TEM was performed, to yield a clear amber, homogeneous solution (in general, no bulk metal was visible by the naked eye at any time unless otherwise indicated). A drop of this solution was then dispersed on a chloroform-cleaned, carbon-coated Cu TEM grid.

Particle Size Measurements. Particle size analysis was performed with the public domain NIH Image 1.62 program developed at the U.S. National Institutes of Health and available on the Internet at http://rsb.info.nih.gov/nih-image/. The details here are identical with those described in the particle size measurement section of ref 5a. Size distributions are quoted as the mean diameter ± standard deviation.

(28) Özkar, S.; Finke, R. G. Molecular Insights for How Preferred Oxoanions Bind to and Stabilize Transition-Metal Nanoclusters: A Tridentate, C_3 Symmetry, Lattice Size-Matching Binding Model. *Coord. Chem. Rev.* **2003** (submitted for publication).

(29) (a) A rough estimate of the metal−metal distance for each of these metals atop their individual nanoclusters, taken as 2 times their bulk-metallic radius,[29b] is as follows: Fe (2.52 Å), Co (2.50 Å), Ni (2.50 Å), Ru (2.68 Å), Rh (2.68 Å), Pd (2.74 Å), Re (2.74 Å), Os (2.70 Å), and Pt (2.78 Å). A 1−4% contraction of these surface distances atop nanoclusters has precedent; see the references and discussion of this point provided elsewhere.[5c] (b) Wells, A. F. *Structural Inorganic Chemistry*; Clarendon Press: Oxford, U.K., 1975; p 1022. For example, the metallic radius of 12-coordinate, fcc-packed Ir is 1.36 Å, so that a first estimate of the Ir−Ir surface distance is twice this value or ca. 2.7 Å, and with even a 4% contraction within the 2.6−2.7 Å range cited in the text.

(30) (a) Day, V. W.; Klemperer, W. G.; Lockledge, S. P.; Main, D. J. *J. Am. Chem. Soc.* **1990**, *112*, 2031. (b) Day, V. W.; Klemperer, W. G.; Main, D. J. *Inorg. Chem.* **1990**, *29*, 2345.

Preparation of $\{(Bu_4N)[(1,5\text{-}C_8H_{12})Ir{\cdot}HPO_4]\}_n$ (1). All manipulations were carried out in the drybox, since complex **1** is moderately air-sensitive. First, 0.183 g (0.540 mmol) of $(Bu_4N)H_2PO_4$ was dissolved in 3 mL of CH_3CN in a 100 mL round-bottomed flask, and then 0.54 mL (0.54 mmol) of 1 M Bu_4NOH aqueous solution was added. The solution was stirred for 3 h and then dried over molecular sieves for 5 h to remove the water. A solution of 0.254 g (0.540 mmol) of $[(1,5\text{-COD})Ir(NCCH_3)_2]BF_4$ in 3 mL of CH_3CN was added to the phosphate solution in the round-bottomed flask, and the final solution was stirred for 3 h. The yellow color of the solution did not change. The volume of the solution was reduced to 2 mL by evaporation under vacuum. The dark-yellow solution was added dropwise into 200 mL of diethyl ether in a beaker. During this addition yellow microcrystals began to precipitate. The stirring was continued for 10 min after the addition. The yellow precipitate, collected over a 35 mL medium glass frit by suction filtration, was redissolved in 2 mL of CH_3CN and transferred into a beaker where 200 mL of diethyl ether was added dropwise while the solution was stirred. The yellow microcrystalline solid precipitated was collected on a 35 mL medium glass frit by suction filtration, washed with 2 × 25 mL of ethyl acetate, and dried under vacuum for 4 h (0.183 g, 0.28 mmol, 53% yield). Washing with ethyl acetate is required to remove excess $Bu_4N^+BF_4^-$ contamination, as determined by ^{19}F NMR spectroscopy, a contamination also easily recognizable from the relative intensities of COD peaks compared to those of Bu_4N^+ peaks in the ^1H NMR spectrum. Anal. Calcd for $C_{24}H_{49}NO_4PIr$: C, 45.11; H, 7.75; N, 2.19; (O, 10.02; P, 4.85; Ir, 30.08). Found (Atlantic Microlab): C, 45.27; H, 7.64; N, 2.22. IR (KBr pellet): 3480 (m, br), 2960 (s), 2874 (s), 1474 (s), 1458 (s), 1204 (s), 1186 (s), 1043 (s), 1014 (s), 567 (w) cm^{-1}. ^1H NMR (300 MHz, CD_3CN, 22 °C): δ (ppm, rel. TMS) 3.48 (CH, m, 2H), 3.30 (CH, m, 20H), 2.31 (*exo*-CH_2, m, 2H), 2.18 (*exo*-CH_2, m, 2H), 1.25 (*endo*-CH_2, m, 4H), 3.10 (N-CH_2, m, 8H), 1.62 (CH_2, m, 8H), 1.38 (CH_2, m, 8H), 0.98 (CH_3, t, 12H), 2.26 ($HOPO_3^-$, br, disappears immediately upon addition of a drop of D_2O into the NMR tube). $^{13}C\{^1H\}$ NMR (75 MHz, CD_3CN, 22 °C): δ (ppm, rel. TMS) 54.707 (=CH), 54.537 (=CH), 32.796 (=CH−CH_2), 32.594 (=CH−CH_2), 59.382 (N−CH_2), 24.441 (CH_2), 20.438 (CH_2), 13.935 (CH_3). $^{31}P\{^1H\}$ NMR (75 MHz, CD_3CN, 22 °C): δ (ppm, relative to 85% H_3PO_4 in a concentric glass capillary internally immersed in the same NMR tube) 14.66. The single ^{31}P NMR peak and the ^1H NMR establish the homogeneity and purity of the complex; the elemental analysis supports the empirical formula $\{[Bu_4N][(1,5\text{-COD})Ir{\cdot}HPO_4]\}_n$, **1**. Negative-ion ES-MS spectrum in acetonitrile gives a main (but not base, nor parent) peak at 493 *m*/*z* with the characteristic isotope distribution for one iridium atom; this peak is assigned to a $[(1,5\text{-COD})Ir(HPO_4)_2]^-$ fragment. Positive-ion ES-MS gives a main peak at 242 *m*/*z* assigned to $[Bu_4N]^+$, but no assignable peaks at higher *m*/*z*. The application of four mass spectroscopy methods [electrospray (ES), fast atom bombardment (FAB), matrix-assisted laser desorption ionization time-of-flight (MALDI-TOF), and chemical ionization (CI)] is suggestive, but was not definitive, of a $n = 2$ formulation in the empirical formula written above; hence, we have retained the more general $n = n$ value for now in formulating **1**. Attempts to crystallize **1** for X-ray structural analysis are continuing.[16] Note that the empirical formula of **1**, plus the fact that the synthesis is simple and reproducible, are both firmly in hand and comprise everything that is needed for the use of **1** in the present work, especially since this complex is reductively disassembled under H_2 en route to HPO_4^{2-}-stabilized Ir(0) nanoclusters. All work reported herein was done with analytically pure **1**.

Air Sensitivity of 1. A 0.036 M solution of **1** in acetonitrile-d_3 in a NMR tube went from yellow to brown in 8 h in air and the 1,5-COD resonances disappeared in the ^1H NMR (but not the Bu_4N^+ butyl group resonances), showing that **1** is mildly air-sensitive as expected from the data for other [(1,5-COD)Ir·polyanion]$^{n-}$ complexes.[30,31] Hence, **1** was stored and manipulated in a N_2-filled Vacuum Atmopsheres drybox that contained ≤1 ppm O_2 by continuous O_2 monitoring.

Hydrogenations. All the nanocluster formation and hydrogenation reactions and kinetics were carried out in the previously described[12,20] custom-built pressurized hydrogenation apparatus utilizing a Fischer−Porter (F−P) pressure bottle. Full details are reported in the Supporting Information.

GLC Determination of the Evolved Equivalents of Cyclooctane during Ir Nanocluster Formation. In the drybox, methylcyclohexane (4 μL; as a GLC internal standard) was added via a 5 μL gastight syringe to a clear, bright-yellow solution of **1** (2.3 mg, 3.6 μmol, 1.2 mM) dissolved in 2.5 mL of acetone plus 0.5 mL of cyclohexene, all placed in a disposable, 1-dram glass vial. A standard conditions (vide infra) hydrogenation reaction was then started in the usual fashion. At the prechosen times indicated by the data in Figure 2, the hydrogen pressure was released and aliquots (≤0.1 mL) of the reaction solution were drawn by use of an 18-in., thoroughly H_2-purged, needle attached to a gastight syringe that had been inserted through the ball valve at the top of the F−P bottle,[12,20] all while under a continuous flow of H_2. Once the aliquot was taken, the F−P bottle was purged an additional five times (15 s/purge) with hydrogen gas and resealed at 40 psig of H_2. The production of cyclooctane vs time is plotted in Figure 2 (right axis).

Curve Fits of Hydrogen Uptake Data and Data Handling. Curve-fitting of the H_2 pressure (or, equivalently, by the 1:1 hydrogen:cyclohexene stoichiometry, the cyclohexene) vs time data was performed, as described previously in detail,[5a,17] by use of the software package Microcal Origin 3.5.4, which is a nonlinear regression subroutine (RLIN) and uses a modified Levenberg−Marquardt algorithm.[32] Details of data handling are available in the Supporting Information. As before,[17] in the uncorrected H_2 pressure vs time curves one observes an initial increase in the pressure due to the equilibration of the solvent vapor pressure after the F−P bottle was flushed with H_2 (15 times, 15 s/purge) before the hydrogenation was started. This vapor pressure increase has been removed, as it should be, from the data used to generate, for example, Figure 1 as well as all the other H_2 pressure vs time data used in this paper. This correction was accomplished as before[5,17] with a control experiment in which the acetone vapor pressure curve is measured independently.

Nanocluster Formation and Cyclohexene Hydrogenations (Standard Conditions). These were performed according to our established protocol; the general procedure is identical to that provided in ref 5a,b. In addition, detailed experimental procedures are provided for individual experiments in the Supporting Information.

General Procedure for Catalyst Lifetime Experiments. Unless otherwise stated, all catalyst lifetime experiments were performed identically to those published previously.[5a,b] In addtion, detailed experimental procedures are provided for individual experiments in the Supporting Information.

Hydrogen Uptake Experiments Beginning with the Precatalyst $\{[Bu_4N][(1,5\text{-COD})Ir{\cdot}HPO_4]\}_n$ (1) Alone (i.e., in the Absence of Cyclohexene). In a drybox, 14.6 mg (2.28×10^{-5} mol) of the precatalyst $\{[Bu_4N][(1,5\text{-COD})Ir{\cdot}HPO_4]\}_n$ (**1**) was weighed into a 2-dram vial and dissolved in 2.0 mL of propylene carbonate that was added via a 5.0 mL gastight syringe, yielding a clear yellow solution. This solution was then transferred via a disposable polyethylene pipet into a reaction flask containing a 3 mm × 10 mm Teflon-coated magnetic stir bar. The reaction flask was sealed, removed from the drybox, and then attached via its sidearm to the gas-uptake apparatus (see Figure K of the Supporting Information in ref 20). Next, the reaction solution was completely degassed (i.e., to $<10^{-4}$ Torr) via three freeze−pump−thaw cycles at liquid nitrogen temperature. Upon final thawing, which was accomplished by submerging the reaction bulb in a plastic cup filled with warm water, the reaction flask was immersed into a water-jacketed vessel thermostated to 22 ± 0.2 °C. Vortex stirring was then initiated and hydrogen gas was introduced as follows: the vacuum line above the sealed reaction bulb was purged by a continuous flow of hydrogen for at least 10 min, and then the reaction solution was thawed for the final time and then sealed. The stopcock connecting the hydrogen tank to the vacuum line was then closed, and the vacuum line itself was reevacuated to $\leq 10^{-4}$ Torr and then sealed by closing the stopcock to the vacuum pump, leaving the vacuum

(31) Pohl, M.; Lyon, D. K.; Mizuno, N.; Nomiya, K.; Finke, R. G. *Inorg. Chem*. **1995**, *34*, 1413 and references therein.

(32) Press, W. H.; Flannery, B. P.; Teukolsky, S. A.; Vetterling, W. T. *Numerical Recipes*; Cambridge University: Cambridge, U.K., 1989.

line under a static vacuum (but not the reaction bulb, which remained closed during this process). The stopcock connecting the hydrogen tank to the vacuum line was then opened, allowing pure hydrogen to fill the vacuum line. Next, the hydrogen pressure in the vacuum line was adjusted to ca. 764 Torr. The stopcock connecting the Baratron to the vacuum line was then closed, sealing a known pressure of hydrogen (ca. 764 Torr) in a known volume ($V_{\text{Baratron}} + V_{\text{arm}}$). The initial millimoles of hydrogen, $n_{\text{hydrogen(initial)}} = 1.47$ mmol, can then be calculated from the ideal gas law, where $P =$ the initial pressure in Torr, $V = 35.58$ mL ($V_{\text{Baratron}} + V_{\text{arm}}$), $T =$ temperature, and $R = 62.36$ mL Torr K^{-1} $mmol^{-1}$.

Next, the reaction solution, still frozen in the sealed reaction bulb, was thawed and brought to room temperature. The reaction bulb was then submerged in a 500 mL water-jacketed reaction flask (22.0 ± 0.2 °C), vortex stirring was initiated, and hydrogen gas was introduced to the solution by opening the stopcock to the reaction bulb. The total pressure in the assembly, $P_{\text{total}} = P_{\text{hydrogen}} + P_{\text{solvent}}$, was then monitored over time via the Baratron pressure transducer. The initial total pressure in this experiment was 154.8 Torr. In a separate, blank experiment under the same conditions with just the propylene carbonate, the solvent vapor pressure of propylene carbonate was determined to be $P_{\text{solvent}} <$ 0.2 Torr at 22 ± 0.2 °C. After 18 h, the reaction flask was sealed by closing the stopcock and transferred into the drybox. The reaction solution was brown after 18 h. Once in the drybox, the flask was opened and the solution was decanted into a screw-cap vial for storage. A 0.2 mL aliquot of the brown solution was sealed in a glass ampule and sent for TEM analysis (Figure S5, Supporting Information). GLC confirmed that 1.0 ± 0.2 equiv of cyclooctane had evolved from the precursor. A total of 2.7 ± 0.5 equiv of hydrogen/mol of iridium was consumed (Figure S4, Supporting Information).

To test the catalytic activity of the iridium(0) nanoclusters, 0.16 mL of this brown solution containing about 3.6 μmol of iridium was drawn via a gastight syringe and added to 2.35 mL of acetone and 0.5 mL (4.94 mmol) of cyclohexene. The resulting brown solution was then transferred via polyethylene pipet to a culture tube and placed inside the F−P bottle, and a hydrogenation run was carried out at 22 °C and beginning with 40 psig of H_2. The cyclohexene hydrogenation reaction proceeded with an induction period of <0.1 h and at an initial rate of 0.6 mmol of H_2/h.

Control Experiment Confirming the Nonreducibility of the $H_2PO_4^-$ Anion under the Nanocluster Formation Reaction Conditions and Detecting Coordination of the $H_2PO_4^-$ to the Nanocluster's Surface by ^{31}P NMR. Recall that the PO_4^{3-} anion and its conjugate acids (HPO_4^{2-}, $H_2PO_4^-$, and H_3PO_4) are relatively stable toward reduction in both acidic and basic solutions due to its large, negative standard reduction potential.[8] In a control reaction, we tested this expected resistance to reduction by H_2 under the reaction conditions used for nanocluster formation and cyclohexene hydrogenation. A solution of **1** (7.2 μmol) and cyclohexene (44 mmol) in 4.5 mL of acetone was subjected to hydrogenation at 22 °C and 40 ± 1 psig of H_2 for 2 days. The solution was dried under vacuum. The residue containing the dihydrogen phosphate anion- and tetrabutylammonium cation-stabilized Ir(0) nanoparticles was dissolved in 0.5 mL of deuterated acetonitrile. The ^{31}P NMR spectrum of this sample shows primarily one broad line (50 Hz width at half-height) centered at 2.5 ppm and relative to an internal capillary of 85% H_3PO_4. For comparison, ^{31}P NMR chemical shifts of $[Bu_4N]H_2PO_4$ and $[Bu_4N]H_2PO_4$ are 4.36 and 5.6 ppm, respectively, of widths at half-height of 1 Hz in deuterated acetonitrile. The chemical shift and broadening of the 2.5 ppm resonance is consistent with dihydrogen phosphate anion interacting with the nanocluster's surface and in fast exchange with free, uncoordinated dihydrogen phosphate. There is also a weak signal at 14.7 ppm in this particular experiment due to the unreacted iridium(I) complex **1** [≤20%; the reaction was not allowed to run to completion in this experiment deliberately to check the integrity of the unreacted precursor Ir(I) complex].

This result shows that neither the HPO_4^{2-} fragment in the precursor complex, **1**, nor the stabilizing $H_2PO_4^-$ anion in the nanoclusters is reduced by hydrogen under the reaction conditions and as the above-cited negative reduction potentials vs H_2 require. More importantly, this experiment demonstrates the promise the ^{31}P handle in $H_2PO_4^-$ holds for future studies of anion-to-nanocluster stabilizing interactions.

Acknowledgment. This work was supported initally by the Department of Energy, Office of Basic Energy Sciences, via DOE Grant FG06-089ER13998, and then by NSF Grant CHE-0078436. A Fulbright Scholar Fellowship to S.Ö. is also gratefully acknowledged.

Supporting Information Available: Extensive experimental details on hydrogenations, data handling, nanocluster formation and cyclohexene hydrogenation, and catalyst lifetime experiments and Figures S1−S17 as described in the text. This information is available free of charge via the Internet at http://pubs.acs.org.

LA0207522